

Figure 1. Chemical structures of known endogenous (1, 2) or synthetic (3–6) RXR agonists.

RXR β and RXR γ (Figure 1).^[11] However, the RXR agonistic activity is much less than that of well-known RXR agonists. The reason for the weak activity is thought to be the introduction of a polar moiety such as a sulfonamide group into the so-called linking group of the common structure of well-known RXR agonists (Figure 2).^[11] In this study, we aimed to develop potent, less-lipophilic and subtype-selective RXR agonists. As a result, we discovered 6-[N-ethyl-N-(3-isopropoxy-4-isopropylphenyl)amino]nicotinic acid (NEt-3IP: 7a) as the first RXR α / β -selective (RXR α / β -dual) agonist. Herein we report the molecular design and in vitro evaluation.

Design strategy

Our previous results suggest that reduction of lipophilicity at the lipophilic domain of RXR agonists enables production of

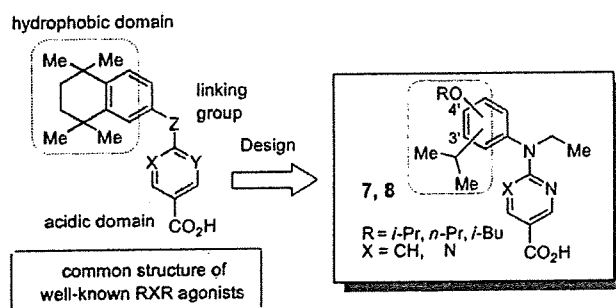


Figure 2. Strategy for the molecular design of subtype-selective RXR agonists possessing alkoxy and isopropyl groups (7, 8).

subtype preference.^[11] To develop potent subtype-selective RXR agonists, we replaced a tetramethyl-cyclohexyl ring, the common hydrophobic domain of well-known RXR agonists, with alkoxy and isopropyl groups, which have more polar characteristics. As it was also found that potent RXR activity requires a lipophilic moiety on the linking amino group,^[11] N-ethylation was performed for moderate lipophilicity. Nicotinic acid or pyrimidine carboxylic acid was applied to the acidic domain (Figure 2).

Chemistry

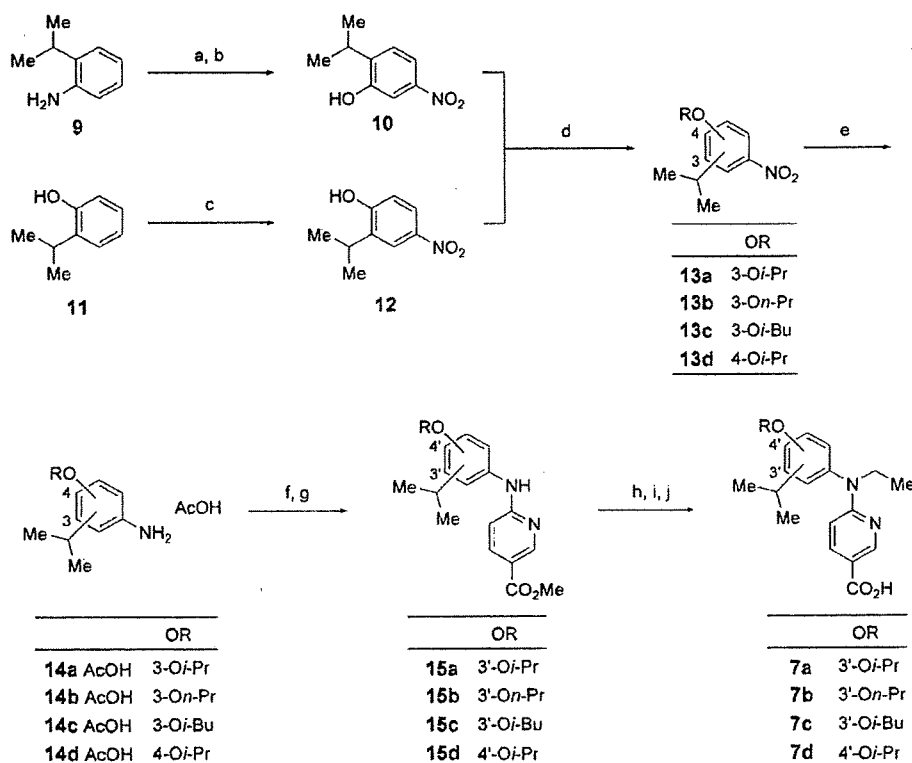
Synthesis was performed by the following steps: synthesis of anilino derivatives, coupling of them with chloronicotinic acid or chloropyrimidine carboxylic acid ester, N-ethylation of the linking amino group, and deprotection of esters. In Scheme 1, synthesis of nicotinic acid derivatives is shown. Anilino derivatives possessing an alkoxy group at the 3-position were prepared by the following procedure: nitration of 2-isopropylaniline with sulfuric acid and nitric acid, replacement of the amino group with a hydroxy group by Sandmeyer reaction, O-alkylation with the corresponding alkyl halide, and hydrogen reduction. On the other hand, anilino derivatives possessing an alkoxy group at the 4-position were prepared from 2-isopropylphenol by radical nitration with nitric acid and zinc chloride in an ultrasonic reactor,^[12] with similar alkylation and reduction to that described above. The anilino derivatives were reacted with 6-chloronicotinic acid in acetic acid, and the carboxyl groups of the products were protected as methyl ester. After N-ethylation of the linking amino group, deprotection of the methyl ester gave the objective compounds 7a–7d.

Compounds 8a and 8c, whose acidic domains are a pyrimidine-5-carboxylic acid, were prepared via the amino intermediates hydrochloride 14a HCl and 14c HCl according to the reported method (Scheme 2).^[13,15] Then N-alkylation and ester deprotection of compounds 16a and 16c were performed to afford the objective compounds 8a and 8c, respectively.

Results and Discussion

RXR agonists alone do not exhibit cell differentiation activity, although they work synergistically with RAR agonists (for example, Am80^[10]) to differentiate the human promyelocyte leukemia cell line HL-60 cells to granulocytes.^[10,15] This phenomenon is based on the synergistic action of RXR with RAR. For the first screening of the compounds, the activity of compounds with RAR agonists (retinoid synergistic activity) were examined with HL-60.^[10,16,17] In this screening, cell differentiation activities were evaluated with nitro blue tetrazolium (NBT) reduction.

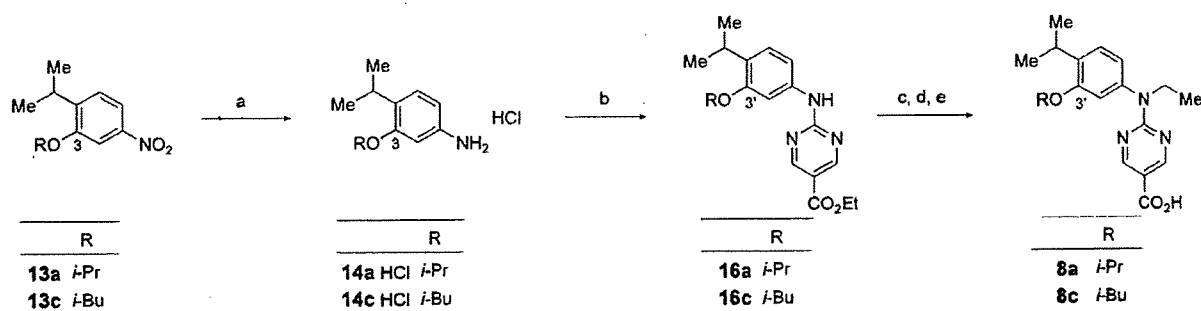
First, to examine the proper position of an alkoxy group on the phenylamino moiety, the retinoid and retinoid synergistic activities of NEt-3IP (7a) and NEt-4IP (7d) were assessed (Table 1). Neither of them showed retinoid activities, suggesting that they do not activate RAR directly. On the other hand, retinoid synergistic activities of 7a and 7d were more potent than or as potent as those of sulfonamide-type RXR agonists



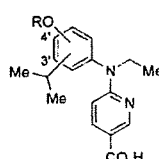
Scheme 1. Reagents and conditions: a) H_2SO_4 , HNO_3 . b) NaNO_2 , H_2SO_4 . c) HNO_3 , EtOAc , ZnCl_2 , u-sonic. d) RX, K_2CO_3 , DMF. e) H_2 , Pd-C, AcOH. f) 6-Chloronicotinic acid, AcOH. g) MeOH, H_2SO_4 . h) EtI, NaH, DMF. i) NaOH, MeOH. j) HCl.

6a and **6b**, respectively (Table 1). These results suggested that application of alkoxy and isopropyl groups to the hydrophobic domain of RXR agonists enables the production of compounds with retinoid synergistic activities. Notably, the retinoid synergistic activity (SEC_{50} value) of NET-3IP (**7a**) is 16 ± 1 nM, which is more effective than that of NET-4IP (**7d**; 135 ± 15 nM). These results prompted us to conclude that the proper position for the introduction of alkoxy is at the 3-position. We therefore investigated the retinoid and retinoid synergistic activities of several derivatives possessing alkoxy groups at the 3-position. NET-3IB (**7c**) possessing a branched alkoxy group, isobutoxy, was found to show potent retinoid synergistic activity without

tween each subtype. For NET-3IP (**7a**), the ratio of EC_{50} (mean values) of RXR α and RXR β to that of RXR γ was more than tenfold, indicating that this compound prefers RXR α/β over RXR γ . On the other hand, for NET-3IB (**7c**) the ratio of EC_{50} (mean values) between RXR α :RXR β :RXR γ was 0.58:23:3, indicating that this compound prefers RXR α over RXR β . As a more than tenfold difference in EC_{50} values generally indicates the existence of selectivity,^[20] it can be assumed that NET-3IP (**7a**) is an RXR α/β -selective agonist (that is, RXR α/β dual agonist). NET-3IB (**7c**) has less subtype selectivity than NET-3IP (**7a**). NET-3IP (**7a**) has comparable RXR potency to representative potent RXR pan agonists, LGD1069 (**3**) and PA024 (**5**), and NET-3IB (**7c**) is



Scheme 2. Reagents and conditions: a) H_2 , Pd-C, MeOH, HCl. b) Ethyl 2-chloro-5-pyrimidinecarboxylic acid, K_2CO_3 , DMF. c) EtI, NaH, DMF. d) NaOH, EtOH. e) HCl.

Table 1. Cell differentiation-inducing activity of compounds 8–10 by NBT reduction assay.^[a]


Compd	OR	Retinoid activity		Retinoid synergist activity	
		EC ₅₀ [nM] ^[b]	BA [%] ^[c]	SEC ₅₀ [nM] ^[d]	BA [%] ^[d]
NET-3IP (7a)	3'-O/Pr	> 1000	n.d. ^[e]	16 ± 1	83 ± 1
NET-3NP (7b)	3'-O <i>n</i> -Pr	> 1000	n.d.	249 ± 16	85 ± 4
NET-3IB (7c)	3'-O/Bu	> 1000	n.d.	25 ± 1	81 ± 2
NET-4IP (7d)	4'-O/Pr	> 1000	n.d.	135 ± 15	77 ± 4
6a ^[d]	–	> 1000	n.d.	309 ± 33	67 ± 5
6b ^[d]	–	> 1000	n.d.	150 ± 17	73 ± 1

[a] All values were determined from full dose-response curves ranging from 10⁻⁹ to 10⁻⁵ M with HL-60 cells. Where errors are indicated, values represent the standard error of the mean value of at least two separate experiments. [b] EC₅₀ or SEC₅₀ was determined as the concentration of a test compound that required to elicit a response at half-maximal height on the dose-response curve. [c] Biological activity (%) is the maximal differentiation ratio that was induced by a test compound. [d] These data were quoted from reference [11]. [e] Not determinable.

more potent than those representative potent RXR pan agonists. PET-3IP (8a) and PET-3IB (8c) showed potent RXR agonistic activities, whereas their subtype selectivity was less than that of NET series compounds. With increasing polarity of the

acidic domain of the compounds, their RXR agonist activity increased but their subtype selectivity decreased. These results were nearly in accordance with the previous report,^[11] suggesting that reduction of the hydrophobic interaction between the hydrophobic domain of the compounds and RXR-ligand binding domain is one strategy to produce subtype selectivity. The CLogP value of NET-3IP (7a) is less than the values of NET-3IB (7c), LGD1069 (3), and PA024 (5). These results indicate that NET-3IP (7a) is a potent, less-lipophilic and subtype-selective RXR agonist.

Conclusions

To develop potent, less lipophilic and subtype-selective RXR agonists, we designed new RXR agonists possessing alkoxy and isopropyl groups as a lipophilic domain of the common structure of well-known RXR agonists. As a result, 6-[*N*-ethyl-*N*-(3-isopropoxy-4-isopropylphenyl)amino]nicotinic acid (NET-3IP: 7a) was discovered as the first RXRα/β-selective agonist. NET-3IP (7a), being potent and having reduced lipophilicity and RXR subtype-selective activity, is expected to become a new medicinal product and to be a useful biological tool for clarifying each RXR subtype function. In the future, to evaluate the effectiveness of the compound, *in vivo* studies such as studies on oral absorption, disposition, toxicity, and anticancer activities are being planned.

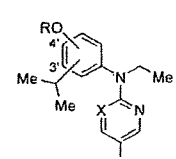
Experimental Section

Chemistry.

Melting points were determined with a Yanagimoto hot-stage melting point apparatus and are uncorrected. IR were recorded on JASCO FT/IR350 (KBr). ¹H NMR spectra were recorded on a VarianVXR-300 (300 MHz) or VarianVXR-500 (500 MHz) spectrometer. Elemental analysis was carried out with a Yanagimoto MT-5 CHN recorder elemental analyzer. FAB-MS was carried out with a VG70-SE.

LGD1069 (3) and PA024 (5). These compounds were prepared according to references <[21] and [13], respectively.

2-Isopropyl-5-nitrophenol (10). Mixed acids (conc. HNO₃ : conc. H₂SO₄ = 2:5, 14 mL) were added to a solution of 2-isopropylaniline 9 (2.7 g, 20 mmol) in conc. H₂SO₄ (8.0 mL) through a dropping funnel with temperature maintained between -5°C and 0°C. The reaction mixture was alkalinized with 2N NaOH and extracted with EtOAc (3 × 200 mL). The organic layer was collected, washed with H₂O (200 mL) and brine

Table 2. Co-transfection data for synthetic compounds and known RXR agonists 3 and 5 in COS-1 cells.^[a]


Compd	OR	X	RXRα		RXRβ		RXRγ		Selectivity ^[e]		CLogP ^f
			EC ₅₀ [nM] ^[b]	E _{max} [%] ^[d]	EC ₅₀ [nM] ^[b]	E _{max} [%] ^[d]	EC ₅₀ [nM] ^[b]	E _{max} [%] ^[d]	β/α	γ/α	
NET-3IP (7a)	3'-O/Pr	CH	32 ± 0	136 ± 11	36 ± 8	115 ± 9	376 ± 13	96 ± 6	1.1	11	5.61
NET-3IB (7c)	3'-O/Bu	CH	0.58 ± 0.02	114 ± 4	23 ± 10	140 ± 13	3 ± 1	103 ± 6	39	5.1	6.23
NET-4IP (7d)	4'-O/Pr	CH	410 ± 40	112 ± 11	1180 ± 210	80 ± 4	1430 ± 30	81 ± 15	2.8	3.4	5.61
PET-3IP (8a)	3'-O/Pr	N	9 ± 2	113 ± 4	36 ± 18	103 ± 3	55 ± 15	105 ± 7	4.0	6.1	4.89
PET-3IB (8c)	3'-O/Bu	N	4 ± 2	106 ± 2	5 ± 0	144 ± 14	4 ± 0	105 ± 13	1.2	1.0	5.50
6a ^[d]	–	–	195 ± 25	115 ± 16	2250 ± 50	52 ± 14	620 ± 50	59 ± 3	11	3.1	6.55
6b ^[d]	–	–	115 ± 5	98 ± 6	635 ± 75	94 ± 2	350 ± 85	81 ± 7	5.5	3.0	6.13
LGD1069 (3)	–	–	3 ± 0	106 ± 12	6 ± 1	114 ± 12	5 ± 2	104 ± 3	2.0	1.6	8.23
PA024 (5) ^[d]	–	–	3 ± 1	–	24 ± 0	–	8 ± 1	–	8.0	2.6	7.23

[a] All values represent the standard error of the mean value of at least two separate experiments with triplicate determinations. [b] EC₅₀ values were determined from full dose-response curves ranging from 10⁻⁹ to 10⁻⁵ M in COS-1 cells. [c] These data were quoted from reference [11]. [d] Luciferase activity of PA024 (5) at 1 μM was defined as 100%. [e] Selectivity was calculated with each EC₅₀ value. [f] CLogP values were calculated with ChemDraw Ultra7.0.

(150 mL), and dried over MgSO_4 . The solvent was evaporated under reduced pressure to yield 2.9 g of 2-isopropyl-5-nitroaniline as brown oil (81%). This compound gave a single spot on TLC, so it was used for the next step without further purification. $^1\text{H NMR}$ (500 MHz, CDCl_3): δ = 7.60 (1 H, dd, J = 8.5, 2.5 Hz), 7.50 (1 H, d, J = 2.5 Hz), 7.24 (1 H, d, J = 8.5 Hz), 3.95 (2 H, br s), 2.90 (1 H, sep, J = 7.0 Hz), 1.29 ppm (6 H, d, J = 7.0 Hz).

NaNO_2 (1.2 g, 18 mmol, dissolved in 3.0 mL of H_2O) was added to a suspension of 2-isopropyl-5-nitroaniline (2.9 g, 16 mmol) in H_2O (3.0 mL) and conc. H_2SO_4 (4.0 mL) with temperature maintained under 5°C . The reaction status was checked by potassium iodide starch test paper. Then the reaction mixture was poured dropwise into a conc. H_2SO_4 (12 mL) and H_2O (9.0 mL) mixture at 120°C . The reaction mixture was poured into H_2O (150 mL) and extracted with EtOAc (3 \times 200 mL). The organic layer was collected, washed with H_2O (200 mL) and brine (150 mL), and dried over MgSO_4 . The solvent was evaporated under reduced pressure. The residue was purified by flash column chromatography (EtOAc : *n*-hexane = 1:5) to yield **10** as brown oil (2.2 g, 75%). $^1\text{H NMR}$ (300 MHz, CDCl_3): δ = 7.78 (1 H, dd, J = 8.5, 2.5 Hz), 7.63 (1 H, d, J = 2.5 Hz), 7.33 (1 H, d, J = 8.5 Hz), 5.80 (1 H, s), 3.31 (1 H, sep, J = 7.0 Hz), 1.28 ppm (6 H, d, J = 7.0 Hz).

2-Isopropoxy-1-isopropyl-4-nitrobenzene (13 a). 2-Bromopropane (0.56 mL, 6.0 mmol), K_2CO_3 (552 mg, 3.6 mmol) and KI (catalytic amount) were added to a solution of **10** (668 mg, 3.7 mmol) in dry DMF (4.0 mL). The reaction mixture was stirred at 70°C for 2 h. Then the reaction mixture was poured into H_2O (80 mL) and extracted with EtOAc (3 \times 80 mL). The organic layer was collected, washed with H_2O (2 \times 80 mL) and brine (80 mL), and dried over MgSO_4 . The solvent was evaporated under reduced pressure. The residue was purified by flash column chromatography to afford **13 a** as light yellow oil (729 mg, 88%). $^1\text{H NMR}$ (500 MHz, CDCl_3): δ = 7.76 (1 H, dd, J = 8.5, 2.0 Hz), 7.66 (1 H, d, J = 2.0 Hz), 7.31 (1 H, d, J = 8.5 Hz), 4.67 (1 H, sep, J = 6.0 Hz), 3.36 (1 H, sep, J = 7.0 Hz), 1.39 (6 H, d, J = 6.0 Hz), 1.22 ppm (6 H, d, J = 7.0 Hz).

1-Isopropyl-4-nitro-2-*n*-propoxybenzene (13 b). 1-Iodopropane (595 mg, 3.5 mmol) and K_2CO_3 (414 mg, 3.0 mmol) were added to a solution of **10** (513 mg, 2.8 mmol) in dry DMF (4.0 mL). The reaction mixture was stirred at 80°C overnight. Then the reaction mixture was poured into H_2O (50 mL) and extracted with EtOAc (3 \times 50 mL). The organic layer was collected, washed with H_2O (2 \times 50 mL) and brine (50 mL), and dried over MgSO_4 . The solvent was evaporated under reduced pressure. The residue was purified by flash column chromatography to yield **13 b** as light yellow oil (426 mg, 68%). $^1\text{H NMR}$ (300 MHz, CDCl_3): δ = 7.80 (1 H, dd, J = 8.5, 2.5 Hz), 7.65 (1 H, d, J = 2.5 Hz), 7.31 (1 H, d, J = 8.5 Hz), 4.02 (2 H, t, J = 6.5 Hz), 3.39 (1 H, sep, J = 7.0 Hz), 1.89 (2 H, m), 1.24 (6 H, d, J = 7.0 Hz), 1.09 ppm (3 H, t, J = 7.5 Hz).

2-Isobutoxy-1-isopropyl-4-nitrobenzene (13 c). Following the procedure to synthesize **13 a**, **13 c** was obtained in 71% yield as clear yellow oil. $^1\text{H NMR}$ (300 MHz, CDCl_3): δ = 7.80 (1 H, dd, J = 8.5, 2.5 Hz), 7.65 (1 H, d, J = 2.5 Hz), 7.32 (1 H, d, J = 8.5 Hz), 3.82 (2 H, d, J = 6.5 Hz), 3.40 (1 H, sep, J = 7.0 Hz), 2.17 (1 H, m), 1.25 (6 H, d, J = 7.0 Hz), 1.08 ppm (6 H, d, J = 6.5 Hz).

3-Isopropoxy-4-isopropylaniline acetate (14 a AcOH). 10% activated Pd-C (catalytic amount) was added to a solution of **13 a** (1.1 g, 4.9 mmol) in AcOH (4.0 mL). The reaction mixture was stirred under H_2 atmosphere at RT for 6 h. The reaction mixture was filtered through celite, and the celite cake was washed with EtOAc (100 mL). The solvent was evaporated under reduced pressure to give **14 a AcOH** (q.y.). This compound gave a single spot on TLC, so it was used for the next step without further purification. $^1\text{H NMR}$ (500 MHz, CDCl_3): δ = 6.96 (1 H, d, J = 8.0 Hz) 6.26 (1 H, dd, J = 8.0,

2.0 Hz), 6.24 (1 H, d, J = 2.0 Hz), 4.46 (1 H, sep, J = 6.0 Hz), 3.19 (1 H, sep, J = 7.0 Hz), 1.32 (6 H, d, J = 6.0 Hz), 1.15 ppm (6 H, d, J = 7.0 Hz).

4-Isopropyl-3-*n*-propoxyaniline acetate (14 b AcOH). Following the procedure to synthesize **14 a AcOH**, **14 b AcOH** was obtained (q.y.). This compound gave a single spot on TLC, so it was used for the next step without further purification. $^1\text{H NMR}$ (300 MHz, CDCl_3): δ = 7.00 (1 H, d, J = 8.0 Hz), 6.36 (1 H, dd, J = 8.0, 2.0 Hz), 6.31 (1 H, d, J = 2.0 Hz), 3.87 (2 H, t, J = 6.5 Hz), 3.22 (1 H, sep, J = 7.0 Hz), 1.81 (2 H, m), 1.17 (6 H, d, J = 7.0 Hz), 1.05 ppm (3 H, t, J = 7.5 Hz).

3-Isobutoxy-4-isopropylaniline acetate (14 c AcOH). Following the procedure to synthesize **14 a AcOH**, **14 c AcOH** was obtained (q.y.). This compound gave a single spot on TLC, so it was used for the next step without further purification. $^1\text{H NMR}$ (300 MHz, CDCl_3): δ = 6.97 (1 H, d, J = 8.0 Hz), 6.27 (1 H, dd, J = 8.0, 2.0 Hz), 6.23 (1 H, d, J = 2.0 Hz), 3.67 (2 H, d, J = 6.5 Hz), 3.22 (1 H, sep, J = 7.0 Hz), 2.10 (1 H, m), 1.18 (6 H, d, J = 7.0 Hz), 1.04 ppm (6 H, d, J = 7.0 Hz).

2-Isopropyl-4-nitrophenol (12). Conc. HNO_3 (2.5 mL, 20 mmol) was added to a solution of 2-isopropylphenol **11** (2.7 g, 20 mmol) in EtOAc (50 mL) in an ice bath. The reaction mixture was placed in an ultrasonic reactor, and ZnCl_2 (3.43 g, 25 mmol) was added in small portions over 2.5 h. The reaction mixture was poured into H_2O (100 mL) and extracted with EtOAc (3 \times 100 mL). The organic layer was collected, washed with H_2O (2 \times 100 mL) and brine (100 mL), and dried over MgSO_4 . The solvent was evaporated under reduced pressure. The residue was purified by flash chromatography to yield **12** (972 mg, 27%) as an off-white solid. $^1\text{H NMR}$ (300 MHz, CDCl_3): δ = 8.13 (1 H, d, J = 3.0 Hz), 8.01 (1 H, dd, J = 9.0, 3.0 Hz), 6.82 (1 H, d, J = 9.0 Hz), 5.74 (1 H, s), 3.25 (1 H, sep, J = 7.0 Hz), 1.30 ppm (6 H, d, J = 7.0 Hz).

1-Isopropoxy-2-isopropyl-4-nitrobenzene (13 d). Following the procedure to synthesize **13 a**, **13 d** was obtained as brown oil (94%). This compound gave a single spot on TLC, so it was used for the next step without further purification. $^1\text{H NMR}$ (300 MHz, CDCl_3): δ = 8.10 (1 H, d, J = 3.0 Hz), 8.07 (1 H, dd, J = 8.5, 3.0 Hz), 6.86 (1 H, d, J = 8.5 Hz), 4.70 (1 H, sep, J = 6.0 Hz), 3.31 (1 H, sep, J = 7.0 Hz), 1.40 (6 H, d, J = 6.0 Hz), 1.24 ppm (6 H, d, J = 7.0 Hz).

4-Isopropoxy-3-isopropylaniline (14 d AcOH). Following the procedure to synthesize **14 a AcOH**, **14 d AcOH** was obtained in crude oil (q.y.). This compound gave a single spot on TLC, so it was used for the next step without further purification. $^1\text{H NMR}$ (300 MHz, CDCl_3): δ = 6.71 (1 H, d, J = 8.5 Hz), 6.64 (1 H, d, J = 3.0 Hz), 6.53 (1 H, dd, J = 8.5, 3.0 Hz), 4.35 (1 H, sep, J = 6.0 Hz), 3.28 (1 H, sep, J = 7.0 Hz), 1.30 (6 H, d, J = 6.0 Hz), 1.17 ppm (6 H, d, J = 7.0 Hz).

4-[*N*-(3-Isopropoxy-4-isopropylphenyl)amino]nicotinic acid methyl ester (15 a). 6-Chloronicotinic acid (788 mg, 5.0 mmol) was added to a solution of **14 a AcOH** (1.24 g, 4.9 mmol) in AcOH (4.0 mL). The reaction mixture was stirred at 80°C for 4 h. The reaction mixture was evaporated under reduced pressure. Conc. H_2SO_4 (catalytic amount) was added to a solution of the residue in dry MeOH (5.0 mL) under ice cooling. The reaction mixture was refluxed overnight. The reaction mixture was poured into sat. NaHCO_3 (100 mL) and extracted with EtOAc (2 \times 50 mL). The organic layer was collected, washed with H_2O (50 mL) and brine (50 mL), and dried over MgSO_4 . The solvent was evaporated under reduced pressure. The residue was purified by flash column chromatography to yield **15 a** (702 mg, 44%). $^1\text{H NMR}$ (300 MHz, CDCl_3): δ = 8.75 (1 H, d, J = 2.5 Hz), 8.08 (1 H, dd, J = 9.0, 2.5 Hz), 7.69 (1 H, br s), 7.19 (1 H, d, J = 8.0 Hz), 6.83 (1 H, d, J = 9.0 Hz), 6.82 (1 H, d, J = 2.0 Hz), 6.81 (1 H, dd, J = 8.0, 2.0 Hz), 4.51 (1 H, sep, J = 6.0 Hz), 3.90 (3 H, s), 3.32 (1 H, sep, J = 7.0 Hz), 1.35 (6 H, d, J = 6.0 Hz), 1.21 ppm (6 H, d, J = 7.0 Hz).

4-[N-(4-Isopropyl-3-*n*-propoxyphenyl)amino]nicotinic acid methyl ester (15b). Following the procedure to synthesize 15a, 15b was obtained as a purple solid (51% for 2 steps). ¹H NMR (300 MHz, CDCl₃): δ = 8.82 (1H, d, *J* = 2.0 Hz), 8.03 (1H, dd, *J* = 9.0, 2.0 Hz), 7.18 (1H, d, *J* = 8.5 Hz), 6.89 (1H, s), 6.85 (1H, d, *J* = 2.0 Hz), 6.84 (1H, dd, *J* = 8.5, 2.0 Hz), 6.79 (1H, d, *J* = 9.0 Hz), 3.91 (2H, t, *J* = 6.5 Hz), 3.88 (3H, s), 3.31 (3H, sep, *J* = 7.0 Hz), 1.84 (2H, m), 1.23 (6H, d, *J* = 7.0 Hz), 1.07 ppm (3H, t, *J* = 7.5 Hz).

4-[N-(3-Isobutoxy-4-isopropylphenyl)amino]nicotinic acid methyl ester (15c). Following the procedure to synthesize 15a, 15c was obtained as purple solid (62% for 2 steps). ¹H NMR (500 MHz, CDCl₃): δ = 8.82 (1H, d, *J* = 2.5 Hz), 8.03 (1H, dd, *J* = 9.0, 2.5 Hz), 7.18 (1H, d, *J* = 8.5 Hz), 6.85 (1H, s), 6.84 (1H, dd, *J* = 8.5, 2.0 Hz), 6.83 (1H, d, *J* = 2.0 Hz), 6.79 (1H, d, *J* = 9.0 Hz), 3.89 (3H, s), 3.71 (2H, d, *J* = 6.5 Hz), 3.32 (1H, sep, *J* = 7.0 Hz), 2.13 (1H, m), 1.23 (6H, d, *J* = 7.0 Hz), 1.06 ppm (1H, d, *J* = 6.5 Hz).

6-[N-(4-Isopropoxy-3-isopropylphenyl)amino]nicotinic acid methyl ester (15d). Following the procedure to synthesize 15a, 15d was obtained as white solid (57% for 2 steps). ¹H NMR (300 MHz, CDCl₃): δ = 8.75 (1H, d, *J* = 2.5 Hz), 8.03 (1H, dd, *J* = 9.0, 2.5 Hz), 7.40 (1H, br s), 7.09 (1H, d, *J* = 3.0 Hz), 7.06 (1H, d, *J* = 8.0, 3.0 Hz), 6.85 (1H, d, *J* = 8.0 Hz), 6.67 (1H, d, *J* = 9.0 Hz), 4.54 (1H, sep, *J* = 6.0 Hz), 3.89 (3H, s), 3.32 (1H, sep, *J* = 7.0 Hz), 1.36 (6H, d, *J* = 6.0 Hz), 1.19 ppm (6H, d, *J* = 7.0 Hz).

4-[N-Ethyl-N-(3-isopropoxy-4-isopropylphenyl)amino]nicotinic acid (7a). 15a (115 mg, 0.35 mmol) was added to a suspension of NaH (16 mg, 0.40 mmol, 60% dispersion in oil) in dry DMF (1.0 mL) at RT under argon. After stirring for 5 min, iodoethane (30 μL, 0.40 mmol) was added, and then it was stirred overnight. The reaction mixture was poured into H₂O (20 mL) and extracted with EtOAc (2 × 10 mL). The organic layer was collected, washed with H₂O (10 mL) and brine (10 mL), and dried over MgSO₄. The solvent was evaporated under reduced pressure to yield a yellow oil. 2N NaOH (0.50 mL) was added to a solution of the residue in MeOH (2.0 mL), and it was stirred at 60 °C for 1 h. The reaction mixture was evaporated under reduced pressure to remove MeOH. The solution was poured into sat. NH₄Cl (20 mL) and extracted with EtOAc (3 × 10 mL). The organic layer was collected, washed with H₂O (2 × 10 mL) and brine (10 mL), and dried over MgSO₄. The solvent was evaporated under reduced pressure. Recrystallization from MeOH afforded 7a as colorless needles (48 mg, 40% for 2 steps). Mp: 212.0–214.0 °C; ¹H NMR (500 MHz, CDCl₃): δ = 8.91 (1H, d, *J* = 2.0 Hz), 7.83 (1H, dd, *J* = 9.0, 2.5 Hz), 7.26 (1H, d, *J* = 8.0 Hz), 6.74 (1H, dd, *J* = 8.0, 2.0 Hz), 6.65 (1H, d, *J* = 2.0 Hz), 6.26 (1H, d, *J* = 9.0 Hz), 4.49 (1H, sep, *J* = 6.0 Hz), 4.06 (2H, q, *J* = 7.0 Hz), 3.32 (1H, sep, *J* = 7.0 Hz), 1.34 (6H, d, *J* = 6.0 Hz), 1.25 (6H, d, *J* = 7.0 Hz), 1.24 ppm (3H, t, *J* = 7.0 Hz); IR (KBr): ν = 1698 cm⁻¹; FAB-MS *m/z*: 343 [M+H]⁺; Anal. Calcd for C₂₀H₂₆N₂O₃: C, 70.15; H, 7.65; N, 8.18. Found: C, 70.18; H, 7.71; N, 8.46.

4-[N-Ethyl-N-(4-isopropyl-3-*n*-propoxyphenyl)amino]nicotinic acid (7b). Following the procedure to synthesize 7a, 7b was obtained as off-white cubics after being recrystallized from CH₂Cl₂/*n*-hexane (62% for 2 steps). Mp: 147.0–148.0 °C; ¹H NMR (300 MHz, CDCl₃): δ = 8.91 (1H, d, *J* = 2.0 Hz), 7.86 (1H, dd, *J* = 9.0, 2.0 Hz), 7.28 (1H, d, *J* = 8.0 Hz), 6.76 (1H, dd, *J* = 8.0, 2.0 Hz), 6.64 (1H, d, *J* = 2.0 Hz), 6.29 (1H, d, *J* = 9.0 Hz), 4.13 (2H, q, *J* = 7.5 Hz), 3.88 (2H, t, *J* = 6.5 Hz), 3.35 (1H, sep, *J* = 7.0 Hz), 1.84 (2H, m), 1.27 (3H, t, *J* = 7.5 Hz), 1.26 (6H, d, *J* = 7.0 Hz), 1.07 ppm (3H, t, *J* = 7.5 Hz); IR (KBr): ν = 2963, 1682 cm⁻¹; FAB-MS *m/z*: 343 [M+H]⁺; Anal. Calcd for C₂₀H₂₆N₂O₃: C, 70.15; H, 7.65; N, 8.18. Found: C, 69.91; H, 7.61; N, 8.13.

4-[N-Ethyl-N-(3-isobutoxy-4-isopropylphenyl)amino]nicotinic acid (7c). Following the procedure to synthesize 7a, 7c was obtained as colorless needles after being recrystallized from CH₂Cl₂/*n*-

hexane (41% for 2 steps). Mp: 191.5–193.0 °C; ¹H NMR (300 MHz, CDCl₃): δ = 8.91 (1H, d, *J* = 2.0 Hz), 7.83 (1H, dd, *J* = 9.0, 2.0 Hz), 7.26 (1H, d, *J* = 8.0 Hz), 6.77 (1H, dd, *J* = 8.0, 2.0 Hz), 6.64 (1H, d, *J* = 2.0 Hz), 6.25 (1H, d, *J* = 9.0 Hz), 4.04 (2H, q, *J* = 7.0 Hz), 3.68 (2H, d, *J* = 6.5 Hz), 3.36 (1H, sep, *J* = 7.0 Hz), 2.12 (1H, m), 1.26 (6H, d, *J* = 7.0 Hz), 1.25 (3H, t, *J* = 7.0 Hz), 1.06 ppm (6H, d, *J* = 6.5 Hz); IR (KBr): ν = 2960, 1684 cm⁻¹; FAB-MS *m/z*: 357 [M+H]⁺; Anal. Calcd for C₂₁H₂₈N₂O₃: C, 70.76; H, 7.86; N, 7.92. Found: C, 70.92; H, 7.90; N, 7.89.

4-[N-Ethyl-N-(4-isopropoxy-3-isopropylphenyl)amino]nicotinic acid (7d). Following the procedure to synthesize 7a, 7d was obtained as off-white cubics after being recrystallized from *n*-hexane (54% for 2 steps). Mp: 212.0–214.0 °C; ¹H NMR (300 MHz, [D₂]DMSO): δ = 12.45 (1H, br s), 8.65 (1H, d, *J* = 2.5 Hz), 7.77 (1H, dd, *J* = 9.0, 2.0 Hz), 7.04 (3H, m), 6.14 (1H, d, *J* = 9.0 Hz), 4.93 (2H, q, *J* = 7.0 Hz), 4.64 (1H, sep, *J* = 6.0 Hz), 3.23 (1H, sep, *J* = 7.0 Hz), 1.31 (6H, d, *J* = 6.0 Hz), 1.15 (6H, d, *J* = 7.0 Hz), 1.14 ppm (3H, t, *J* = 7.0 Hz); IR (KBr): ν = 1664 cm⁻¹; FAB-MS *m/z*: 343 [M+H]⁺; Anal. Calcd for C₂₀H₂₆N₂O₃: C, 70.15; H, 7.65; N, 8.18. Found: C, 70.02; H, 7.36; N, 8.23.

3-Isopropoxy-4-isopropylaniline hydrochloride (14a HCl). 10% activated Pd-C (catalytic amount) was added to a solution of 13a (1880 mg, 8.4 mmol) in MeOH (15 mL). The reaction mixture was stirred under H₂ atmosphere at RT for 4 h. The reaction mixture was filtered through celite, and the celite cake was washed with MeOH. The solution was concentrated under reduced pressure. Conc. HCl (0.5 mL) and EtOAc (30 mL) were added to the concentrated solution. The precipitate was filtered to give colorless needles (1915 mg). Following the procedure to synthesize 14a HCl, 14c HCl was obtained as colorless needles (89%). ¹H NMR (300 MHz, CDCl₃): δ = 9.84 (2H, br s), 7.23 (1H, d, *J* = 8.0 Hz), 6.89 (1H, s), 6.81 (1H, d, *J* = 8.0 Hz), 4.53 (1H, sep, *J* = 6.0 Hz), 3.19 (1H, sep, *J* = 7.0 Hz), 1.30 (6H, d, *J* = 6.0 Hz), 1.14 ppm (d, *J* = 7.0 Hz).

3-Isobutoxy-4-isopropylaniline hydrochloride (14c HCl). Following the procedure to synthesize 14a HCl, 14c HCl was obtained as colorless needles (89%). ¹H NMR (300 MHz, CDCl₃): δ = 6.98 (2H, br s), 7.23 (1H, d, *J* = 8.0 Hz), 6.81 (1H, s), 6.80 (1H, d, *J* = 8.0 Hz), 3.73 (2H, d, *J* = 6.5 Hz), 3.22 (1H, sep, *J* = 6.5 Hz), 2.08 (1H, m), 1.16 (6H, d, *J* = 6.5 Hz), 1.02 ppm (6H, d, *J* = 6.5 Hz).

2-[N-(4-Isopropoxy-3-isopropylphenyl)amino]pyrimidine-5-carboxylic acid ethyl ester (16a). K₂CO₃ (622 mg, 4.5 mmol) and DMF (5 drops) were added to a mixture of 2-chloropyrimidine-5-carboxylate (120 mg, 0.60 mmol) and 14a HCl (148 mg, 0.60 mmol). The mixture was stirred at 120 °C for 12 h. The mixture was poured into 2N HCl (30 mL) and extracted with EtOAc (2 × 30 mL). The organic layer was collected, washed with H₂O (2 × 30 mL) and brine (20 mL), and dried over MgSO₄. The solvent was evaporated under reduced pressure. The residue was purified by flash column chromatography (EtOAc:*n*-hexane = 1:6) to yield 16a (152 mg, 69%) as a colorless solid. ¹H NMR (500 MHz, CDCl₃): δ = 8.95 (2H, s), 7.39 (1H, br s), 7.34 (1H, d, *J* = 2.0 Hz), 7.16 (1H, d, *J* = 8.0 Hz), 6.99 (1H, dd, *J* = 8.0, 2.0 Hz), 4.56 (1H, sep, *J* = 6.0 Hz), 4.37 (2H, q, *J* = 7.0 Hz), 3.28 (1H, sep, *J* = 7.0 Hz), 1.39 (3H, t, *J* = 7.0 Hz), 1.37 (6H, d, *J* = 6.0 Hz), 1.20 ppm (6H, d, *J* = 7.0 Hz).

2-[N-(4-Isobutoxy-3-isopropylphenyl)amino]pyrimidine-5-carboxylic acid ethyl ester (16c). Following the procedure to synthesize 16a, 16c was obtained as a colorless solid (33%). ¹H NMR (300 MHz, CDCl₃): δ = 8.95 (2H, s), 7.46 (1H, s), 7.26 (1H, d, *J* = 2.5 Hz), 7.17 (1H, d, *J* = 8.5 Hz), 7.03 (1H, dd, *J* = 8.5, 2.5 Hz), 4.38 (2H, q, *J* = 7.0 Hz), 3.76 (2H, d, *J* = 6.5 Hz), 3.31 (1H, m), 2.44 (1H, sep), 1.39 (3H, t, *J* = 7.0 Hz), 1.22 (6H, d, *J* = 7.0 Hz), 1.07 ppm (6H, d, *J* = 7.0 Hz).

2-[N-Ethyl-N-(4-isopropoxy-3-isopropylphenyl)amino]pyrimidine-5-carboxylic acid (8a). A solution of 16a (40 mg, 0.12 mmol) was added to a suspension of NaH (8 mg, 0.20 mmol) in DMF (2.0 mL)

under Ar atmosphere. The solution was stirred at RT for 10 min, and then EtI (10 μ L, 0.12 mmol) was added, and stirring was continued for an additional 10 min. The solution was poured into H₂O (20 mL) and extracted with EtOAc (2 \times 15 mL). The organic layer was collected, washed with H₂O (2 \times 20 mL) and brine (10 mL), and dried over MgSO₄. The solvent was evaporated to yield 38 mg of colorless solid. 2 N NaOH (2.0 mL) was added to a solution of the residue (35 mg, 0.10 mmol) in EtOH (2.0 mL). The mixture was stirred at 60 °C for 10 min. The solution was neutralized with 2 N HCl and extracted with EtOAc (2 \times 15 mL). The organic layer was collected, washed with H₂O (2 \times 20 mL) and brine (10 mL), and dried over MgSO₄. The solvent was evaporated under reduced pressure to yield **8a** (32 mg, 88% for 2 steps) as a colorless solid. Mp: 197.5–199.0 °C; ¹H NMR (300 MHz, CDCl₃): δ = 8.74 (2H, s), 7.21 (1H, d, *J* = 8.0 Hz), 6.83 (1H, d, *J* = 2.0 Hz), 6.77 (1H, dd, *J* = 8.0, 2.0 Hz), 4.56 (1H, sep, *J* = 6.0 Hz), 4.00 (2H, q, *J* = 7.0 Hz), 2.11 (1H, sep, *J* = 7.0 Hz), 1.26 (6H, d, *J* = 6.0 Hz), 1.19 (6H, d, *J* = 7.0 Hz), 1.16 ppm (3H, t, *J* = 7.0 Hz); IR (KBr): ν = 1674 cm⁻¹; FAB-MS *m/z*: 344 [M + H⁺]; Anal. Calcd for C₁₉H₂₅N₃O₃: C, 66.45; H, 7.34; N, 12.24. Found: C, 66.38; H, 7.29; N, 12.43.

2-[N-Ethyl-N-(4-isobutoxy-3-isopropylphenyl)amino]pyrimidine-5-carboxylic acid (8c). Following the procedure to synthesize **8a**, **8c** was obtained as colorless needles (69% for 2 steps). Mp: 180.5–182.0 °C; ¹H NMR (300 MHz, CDCl₃): δ = 8.89 (2H, s), 7.26 (1H, d, *J* = 8.0 Hz), 6.79 (1H, dd, *J* = 8.0, 2.0 Hz), 6.66 (1H, d, *J* = 2.0 Hz), 4.06 (2H, q, *J* = 7.0 Hz), 3.69 (2H, d, *J* = 6.5 Hz), 3.34 (1H, m), 2.11 (1H, sep), 1.28 (3H, t, *J* = 7.0 Hz), 1.25 (6H, d, *J* = 7.0 Hz), 1.05 ppm (6H, d, *J* = 6.5 Hz); IR (KBr): ν = 1673 cm⁻¹; Anal. Calcd for C₂₀H₂₇N₃O₃: C, 67.20; H, 7.61; N, 11.76. Found: C, 67.01; H, 7.25; N, 11.60.

Calculation of CLogP Values. LogP values for compounds were calculated with ChemDraw Ultra 7.0.

NBT Reduction Assay

Culture of HL-60 cells. The human promyelocyte leukemia cell line HL-60 was cultured in RPMI1640, which contained 10% fetal bovine serum (FBS) and antibiotics (2% of penicillin-streptomycin solution purchased from SIGMA), in a humidified atmosphere of 5% CO₂ at 37 °C.

NBT reduction assay.^[10,16,17] Test compounds were dissolved in DMSO at 20 mM for stock solutions. A test compound solution in DMSO was added to a suspension of cells at a concentration of 8 \times 10⁴ cells mL⁻¹. Final DMSO concentration was kept below 0.1%. For vehicle and positive controls, the same volume of DMSO and Am80^[8] solution in DMSO were added, respectively. After incubation for 4 days, NBT reduction assay was performed as described below. Cells were incubated in RPMI1640 (10% FBS) and an equal volume of phosphate-buffer saline (PBS (-)) containing 0.2 w/w% NBT and 12-*O*-tetradecanoylphorbol-13-acetate (TPA, 200 ng mL⁻¹) in a humidified atmosphere of 5% CO₂ at 37 °C for 30 min. The rate of cell differentiation was calculated by the percentage of cells containing blue-black formazan using more than 200 cells. The average of at least three results for each assay was calculated. Synergistic activities of test compounds with Am80 were evaluated in the presence of 3.3 \times 10⁻¹⁰ M of Am80, which induces less than 10% of cell differentiation, according to the method described above.

Luciferase Reporter Gene Assay

Culture of COS-1 cells. COS-1 cells were maintained in Dulbecco's modified Eagle's medium supplemented with 10% FBS in a humidified atmosphere of 5% CO₂ at 37 °C.

Luciferase reporter gene assay.^[13,18,19] Luciferase reporter gene assays were performed using COS-1 cells transfected with three kinds of vectors: each RXR subtype, a luciferase reporter gene under the control of the appropriate RXR response elements, and secreted alkaline phosphatase (SEAP) gene as a background. A CRBPII-tk-Luc reporter and plasmid DNA was purified by a QIA filter Plasmid Midi kit. COS-1 cells were transfected with QIA Effectene Transfection reagent according to the supplier's protocol. Test compound solutions whose DMSO concentrations were below 1% were added to the suspension of transfected cells, which were seeded at about 4 \times 10⁴ cells mL⁻¹ in 96-well white plates. For vehicle and positive controls, the same volume of DMSO and 9-*cis*RA solution in DMSO were added, respectively. After incubation in a humidified atmosphere of 5% CO₂ at 37 °C for 18 h, some of the medium was used for SEAP and the remaining cells were used for luciferase reporter gene assays with a Steady-Glo Luciferase Assay system (Promega) according to the supplier's protocol. The luciferase activities were normalized using secreted alkaline phosphatase (SEAP) activities. The assays were carried out in duplicate three times.

Acknowledgements

The authors are grateful to the SC NMR Laboratory of Okayama University for the NMR experiment. This research was partially supported by a Grant-in Aid for Scientific Research on Priority Areas from the Ministry of Education, Science, Culture and Sports of Japan (No. 17790090), by the subsidy to promote science and technology in the prefectures where nuclear power plants and other power plants are located, and by a grant from the Research on Nanotechnical Medical of the Japan Health Sciences Foundation and Health and Labour Sciences Research Grants (HLSRG).

Keywords: cell differentiation · dual agonist · RXR agonists · subtype selective · synergistic effect

- [1] L. Altucci, M. D. Leibowitz, K. M. Ogilvie, A. R. D. Lera, H. Gronemeyer, *Nat. Rev. Drug. Discov.* **2007**, *6*, 793–810.
- [2] A. R. de Lera, W. Bourguet, L. Altucci, H. Gronemeyer, *Nat. Rev. Drug. Discov.* **2007**, *6*, 811–820.
- [3] C. J. Grubbs, D. L. Hill, K. I. Bland, S. W. Beenken, T.-H. Lind, I. Eto, V. R. Atigadda, K. K. Vines, W. J. Brouillette, D. D. Muccio, *Cancer Lett.* **2003**, *201*, 17–24.
- [4] W.-C. Yen, M. R. Corpuz, R. Y. Prudente, T. A. Cooke, R. P. Bissonnette, A. Negro-Vilar, W. W. Lamph, *Clin. Cancer Res.* **2004**, *10*, 8656–8664.
- [5] V. Giguère, *Endocr. Rev.* **1999**, *20*, 689–725.
- [6] D. J. Mangelsdorf, C. Thummel, M. Beato, P. Herrlich, G. Schütz, K. Umesono, B. Blumberg, P. Kastner, M. Mark, P. Chambon, R. M. Evans, *Cell* **1995**, *83*, 835–839.
- [7] D. J. Mangelsdorf, R. M. Evans, *Cell* **1995**, *83*, 841–850.
- [8] A. Szanto, V. Narkar, Q. Shen, I. P. Uray, P. J. A. Davies, L. Nagy, *Cell Death Differ.* **2004**, *11*, S126–S143.
- [9] P. F. Egea, A. Mitschler, D. Moras, *Mol. Endocrinol.* **2002**, *16*, 987–997.
- [10] H. Kagechika, K. Shudo, *J. Med. Chem.* **2005**, *48*, 5875–5883.
- [11] K. Takamatsu, A. Takano, N. Yakushiji, K. Morishita, N. Matsuura, M. Makishima, H. I. Ali, E. Akaho, A. Tai, K. Sasaki, H. Kakuta, *ChemMedChem*, in press.
- [12] A. Kamal, B. A. Kumar, M. Arifuddin, M. Patrick, *Ultrasonics Sonochemistry* **2004**, *11*, 455–457.
- [13] K. Ohta, E. Kawachi, N. Inoue, H. Fukasawa, Y. Hashimoto, A. Itai, H. Kagechika, *Chem. Pharm. Bull.* **2000**, *48*, 1504–1513.

- [14] A. Takamizawa, K. Tokuyama, H. Satoh, *Yakugaku Zasshi* 1959, 79, 664–669.
- [15] L. Nagy, V. A. Thomázy, G. L. Shipley, L. Fésüs, W. Lamph, R. A. Heyman, R. A. S. Chandraratna, P. J. A. Davies, *Mol. Cell. Biol.* 1995, 15, 3540–3551.
- [16] S. J. Collins, F. W. Ruscetti, R. E. Gallagher, R. C. Gallo, *J. Exp. Med.* 1979, 149, 969–974.
- [17] T. Takuma, K. Takeda, K. Konno, *Biochem. Biophys. Res. Commun.* 1987, 145, 514–521.
- [18] K. Umesono, K. K. Murakami, C. C. Thompson, R. M. Evans, *Cell* 1991, 65, 1255–1266.
- [19] S. R. Kain, *Methods Mol. Biol.* 1997, 63, 49–60.
- [20] L. Ye, Y.-L. Li, K. Mellström, C. Mellin, L. G. Bladh, K. Koehler, N. Garg, A. M. G. Collazo, C. Litten, B. Husman, K. Persson, J. Ljunggren, G. Grover, P. G. Sleph, R. George, J. Malm, *J. Med. Chem.* 2003, 46, 1580–1588.
- [21] M. F. Boehm, L. Zhang, B. A. Badea, S. K. White, D. E. Mais, E. Berger, C. M. Suto, M. E. Goldman, R. A. Heyman, *J. Med. Chem.* 1994, 37, 2930–2941.

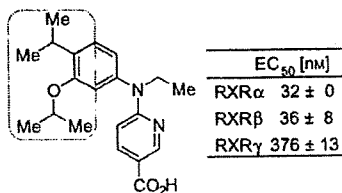
Received: November 2, 2007

Revised: January 16, 2008

Published online on ■■■ ■■, 2008

FULL PAPERS

The first subtype-selective RXR agonist. NEt-3IP (7a) was found to be the first RXR α / β -selective (or RXR α / β -dual) agonist. Being potent, less lipophilic than previous agonists, and having RXR subtype-selective activity, NEt-3IP (7a) is expected to become a new drug candidate and to be a useful biological tool for clarifying each RXR subtype function.



7a (NEt-3IP): RXR α / β -selective agonist

K. Takamatsu, A. Takano, N. Yakushiji, K. Morohashi, K.-i. Morishita, N. Matsuura, M. Makishima, A. Tai, K. Sasaki, H. Kakuta*



The First Potent Subtype-Selective Retinoid X Receptor (RXR) Agonist Possessing a 3-Isopropoxy-4-isopropylphenylamino Moiety, NEt-3IP (RXR α / β -dual agonist)



Albumin-conjugated PEG liposome enhances tumor distribution of liposomal doxorubicin in rats

Jun-ichi Yokoe^{a,b}, Shiho Sakuragi^a, Kayoko Yamamoto^a, Takuya Teragaki^b, Ken-ichi Ogawara^b, Kazutaka Higaki^b, Naohisa Katayama^a, Toshiya Kai^a, Makoto Sato^a, Toshikiro Kimura^{b,*}

^a Pharmaceutical Research Division, NIPRO Corporation, Shiga 525-0055, Japan

^b Department of Pharmaceutics, Faculty of Pharmaceutical Sciences, Okayama University, 1-1-1 Tsushima-Naka, Okayama 700-8530, Japan

Received 24 July 2007; received in revised form 3 November 2007; accepted 6 November 2007

Available online 13 November 2007

Abstract

To evaluate the effect of coupling of recombinant human serum albumin (rHSA) onto the surface of poly(ethylene glycol)-modified liposome (PEG liposome) on the *in vivo* disposition characteristics of liposomal doxorubicin (DXR), the pharmacokinetics and tissue distribution of DXR were evaluated after intravenous administration of rHSA-modified PEG (rHSA/PEG) liposomal DXR into tumor-bearing rats. rHSA/PEG liposome prepared using a hetero-bifunctional cross-linker, *N*-succinimidyl 3-(2-pyridyldithio) propionate (SPDP), efficiently encapsulated DXR (over 95%). rHSA/PEG liposomal DXR showed longer blood-circulating property than PEG liposomal DXR and the hepatic and splenic clearances of rHSA/PEG liposomal DXR were significantly smaller than those of PEG liposomal DXR. It was also demonstrated that the disposition of DXR to the heart, one of the organs for DXR-related side-effects, was significantly smaller than free DXR. Furthermore, the tumor accumulation of rHSA/PEG liposomal DXR was significantly larger than that of PEG liposomal DXR. The “therapeutic index”, a criterion for therapeutic outcome, for rHSA/PEG liposomal DXR was significantly higher than PEG liposomal DXR. These results clearly indicate that rHSA-conjugation onto the surface of PEG liposome would be a useful approach to increase the effectiveness and safety of PEG liposomal DXR.

© 2007 Elsevier B.V. All rights reserved.

Keywords: Recombinant human serum albumin (rHSA); PEG liposome; Doxorubicin; Tumor-bearing rats; Passive targeting

1. Introduction

Liposomes containing either monosialoganglioside GM1 (Allen et al., 1989) or polyethylene glycol (PEG) derivatives (Blume and Cevc, 1990; Klibanov et al., 1990; Allen et al., 1991; Maruyama et al., 1992; Woodle and Lasic, 1992; Yuda et al., 1996) are not readily taken up by the macrophages in reticuloendothelial system (RES), and hence remain in the blood circulation for a relatively long period of time. Particularly, PEG-modified liposomes (PEG liposomes) have been utilized as a particulate carrier for anti-tumor therapy due to their long circulation time. Generally, as the capillary permeability of the endothelium in newly vascularized tumors is significantly greater than that of normal organs, long-circulating PEG liposomes are preferentially delivered and accumulated into the

tumors (enhanced permeability and retention (EPR) effect), which provides a great opportunity for passive targeting of liposomal anticancer agents into tumor tissues (Maeda et al., 2000; Luigi et al., 2003).

Doxorubicin hydrochloride (DXR) is the most commonly used anthracycline and is one of the most active agents in the treatment of breast cancer. However, it sometimes causes cardiotoxicity, which could lead to congestive heart failure and death (Dresdale et al., 1983; Speth et al., 1988). One of the approaches to avoid DXR-related toxicity is to encapsulate it into appropriate drug carriers, which provides a change in the *in vivo* distribution of DXR, resulting in reduced DXR levels in the heart (Abraham et al., 2005). DXR encapsulated in PEG liposome, known as Doxil in the United States, has revealed an increased therapeutic efficacy and reduced cardiotoxicity compared to free DXR (Working and Dayan, 1996; Gabizon et al., 2003).

In the previous study, we reported that rat serum albumin (RSA)-conjugated PEG liposomes showed the longer circula-

* Corresponding author. Tel.: +81 86 251 7948; fax: +81 86 251 7926.
E-mail address: kimura@pharm.okayama-u.ac.jp (T. Kimura).

tion time than PEG liposomes after intravenous administration into rats (Furumoto et al., 2007), suggesting the potential of the albumin-conjugated PEG liposomes as a suitable carrier for various anticancer drugs. Albumin is one of the endogenous, non-toxic, non-immunogenic and relatively hydrophilic proteins in the body. Its introduction on the surface of liposomes reduced the association of serum proteins including some given serum opsonins onto the surface, resulting in the more prolonged circulation time of PEG liposome (Furumoto et al., 2007). However, since the conjugation of rat serum albumin onto PEG liposome with carbodiimide has to be conducted under weakly acidic condition, the pH remote loading method (Mayer et al., 1986; Madden et al., 1990), which can encapsulate DXR into the liposome very efficiently, was not available. In the present study, we changed the method for albumin conjugation in order to encapsulate DXR into liposomes by utilizing the pH remote loading method. *N*-Succinimidyl 3-(2-pyridyldithio) propionate (SPDP) (Carlsson et al., 1978) was selected as a hetero-bifunctional cross-linking agent to couple recombinant human serum albumin (rHSA) onto PEG liposome. This method allowed us to employ the pH remote loading of DXR into the liposome. Then, the effect of rHSA-conjugation to PEG liposome was evaluated in terms of pharmacokinetics and biodistribution of liposomal DXR in Yoshida sarcoma (LY-80)-bearing rats.

2. Materials and methods

2.1. Materials

Egg phosphatidylcholine (egg PC) was purchased from ASAHI KASEI Chemicals Industry Inc. (Tokyo, Japan). Cholesterol (Chol), doxorubicin hydrochloride (DXR) and daunorubicin hydrochloride were obtained from Wako Pure Chemical Industry Inc. (Osaka, Japan). Dioleoyl phosphatidylethanolamine (DOPE) and distearoylphosphatidylethanolamine-*N*-[methoxy poly (ethylene glycol)-2000] (PEG-DSPE) were purchased from NOF Inc. (Tokyo). SPDP was purchased from PIERCE Inc. (Rockford, IL, USA). rHSA was gifted from Bipla Inc. (Chitose, Japan).

2.2. Synthesis of PDP-DOPE₂ as a linker of rHSA-conjugation with liposomes

We synthesized a DOPE derivatized with terminal pyridyldithiopropionate (PDP) groups as previously reported (Barbet et al., 1981; Ishimori et al., 1984). Mixture of DOPE in chloroform and SPDP in methanol (SPDP:DOPE = 67.2:78 molar ratio) were stirred for 2 h under nitrogen gas at room temperature after a small aliquot of triethylamine was added to the mixture. To remove unreacted SPDP, the organic phase was reverse-extracted with phosphate-buffered saline (PBS, pH 7.4) three times. After the organic solvent was evaporated, the residue was re-dissolved in chloroform to give a final concentration of 10 μ mol PDP-DOPE/mL. Thin layer chromatography (solvent; chloroform:methanol:water = 65:25:4 molar ratio) on silica gel indicated a single spot under UV illumination.

2.3. Preparation of liposomes

Liposomes were prepared according to the following procedures. Lipid mixture (Egg PC:Chol:PEG-DSPE:PDP-DOPE = 61:30:5:4 molar ratio) was dried by rotary evaporator at 40 °C. Two hundred and fifty mM ammonium sulfate solution (pH 5.5) was added to the thin-film of lipids and the mixture was hydrated at 60 °C. The resultant suspension was extruded at least 10 times through polycarbonate membranes of 100 nm pore size (Whatman plc., Brentford, UK). External solution was replaced with PBS (pH 8.0) by gel filtration with a Sephadex G-25 column (PD-10, GE Healthcare Ltd., Buckinghamshire, UK).

DXR was encapsulated into liposome using the pH remote loading method (Bolotin et al., 1994). DXR was dissolved at 7 mg/mL in PBS (pH 8.0), and then, immediately mixed with liposomal suspension and incubated at 60 °C for 1 h. Non-encapsulated DXR was removed with a PD-10 column equilibrated with PBS (pH 8.0). The extent of DXR encapsulation was determined by measuring liposomal DXR amount by HPLC method as described below.

2.4. Coupling of PDP-rHSA to liposomes

SPDP in methanol was added to rHSA dissolved in PBS (SPDP:rHSA = 20:1 molar ratio) under nitrogen gas and the mixture was incubated at room temperature for 30 min. Excess of SPDP was then removed by Sepharose CL-6B column (Bio-Rad, Emeryville, CA) equilibrated with acetate buffer (pH 4.5). PDP-rHSA was incubated with dithiothreitol (DTT) (PDP-rHSA:DTT = 1:250 molar ratio) for 20 min at room temperature and the reaction mixture was applied to a Sepharose CL-6B column equilibrated with PBS (pH 8.0) to remove unreacted DTT. The activated rHSA in the elution was dropped to liposomal suspensions and the mixture was left at least for 18 h at room temperature under nitrogen gas with gentle stirring. Unreacted rHSA was removed by Sepharose CL-6B column equilibrated with PBS (pH 8.0). As a control, "PEG liposome" was also prepared by coupling cysteine instead of rHSA.

2.5. Physicochemical characterization of rHSA-conjugated PEG liposomes (rHSA/PEG liposomes) encapsulating DXR

The diameter of the liposomes was determined by light-scattering spectroscopy using a NICOMP zls-370 (Particle Sizing System, Santa Barbara, CA). Lipid and rHSA amounts were estimated by using Phospholipid B test Wako and albumin test Wako (Wako Pure Chemical Industries, Osaka), respectively. Each liposome sample was subjected to SDS-polyacrylamide gel electrophoresis (SDS-PAGE) as previously reported (Furumoto et al., 2007).

In vitro stability of liposome encapsulating DXR was tested as follows: DXR-encapsulated liposomal suspensions were incubated with the same volume of rat plasma at 37 °C for 2 h. Then, the released DXR was separated by the Sepharose CL-6B column and was determined spectrofluorometrically (Ex = 500 nm, Em = 550 nm).

2.6. Determination of the amount of serum proteins associated with liposomes

Liposomes were incubated in rat serum (liposomal suspension:serum = 1:1, v/v) for 20 min at 37 °C, and subsequently bulk serum proteins were removed by Sepharose CL-4B column (Bio-Rad, Emeryville, CA). The amount of serum proteins associated with liposomes was calculated by subtracting the amount of rHSA coupled with liposomes from the amount of total protein quantified by Lowry's method (Lowry et al., 1951).

2.7. Animals

Male Donryu rats weighing 200–280 g (Charles River Laboratories Inc., Yokohama, Japan) were used throughout the present study. Rats were maintained at 23 °C and 55% of humidity with free access to standard rat food and water. Our investigations were performed after approval by our local ethical committee at Nipro Corporation and Okayama University, and in accordance with Principles of Laboratory Animal Care (NIH publication #85-23).

2.8. In vivo disposition experiments

LY-80, rat ascites sarcoma cell line was kindly provided from Cell Resource Center for Biomedical Research, Institute of Development, Aging and Cancer, Tohoku University (Sendai, Japan). Rats were subcutaneously inoculated into the thigh with 1.0×10^6 LY-80 cells in a volume of 0.1 mL. Liposomal DXR or free DXR was intravenously injected at 2.0 mg/kg as DXR around 7 days after the tumor inoculation, when the tumor grew up to about 600 mm³ in volume. Then, blood samples were periodically taken from the cannulated jugular vein. Blood samples (0.2 mL) were centrifuged immediately at $4000 \times g$ for 5 min and the obtained plasma samples were kept at –20 °C until analysis. Tissue distribution studies were conducted as follows. At 3 h after intravenous injection, organs (liver, spleen, heart and tumor) were excised, rinsed with PBS and weighed. All tissues were stored at –20 °C until analysis.

2.9. Analytical method

DXR was extracted from plasma and tissue samples as previously reported (Bally et al., 1990; Embree et al., 1993). In brief, 0.1 mL of plasma was added to 0.9 mL of saturated ammonium sulfate (pH 4.0 buffered saline) with daunorubicin, an internal standard. Subsequently, the sample was extracted with 2 mL of chloroform/isopropanol (1:1, v/v). Following vigorous mixing, $1600 \times g$ -centrifugation and the evaporation of organic phase, the residue was re-dissolved in HPLC mobile phase. In the case of tissue samples, after each tissue was homogenized with PBS (pH 7.4) (3.0 g/mL), 1 mL of the homogenate was subjected to the same procedure used for plasma samples.

The HPLC system was composed of LC-10AS pump, SIL-10A autosampler, RF-10A fluorescence detector (Shimadzu, Kyoto, Japan) set at $\lambda_{\text{ex}} = 500$ nm and $\lambda_{\text{em}} = 550$ nm. An ODS column (5C₁₈, 150 mm \times 4.6 mm i.d., Nacal Tesque, Inc., Kyoto)

was used at room temperature. The mobile phase was 1/15 M KH₂PO₄:CH₃CN = 75:25 (v/v, pH 4.16, adjusted with H₃PO₄), which was delivered at 1.0 mL/min. The coefficient of variation (CV) for standard curves ranged from 2.3 to 5.6 and the squared correlation coefficient was over 0.99.

2.10. Pharmacokinetic analysis

Plasma concentrations of DXR (C_p) versus time curves were analyzed by Eq. (1) using the non-linear least-square regression program MULTI (Yamaoka et al., 1981)

$$C_p = A e^{-\alpha t} + B e^{-\beta t} \quad (1)$$

The area under the plasma concentration–time curve (AUC) was calculated by the following equation:

$$\text{AUC} = \int_0^t C_p dt \quad (t = \infty) \quad (2)$$

Tissue clearance (CL_{tissue}) was calculated by the following equation:

$$CL_{\text{tissue}} = \frac{X_0^t}{\text{AUC}_0^t} \quad (t = 3 \text{ h}) \quad (3)$$

where AUC_0^t means AUC value from 0 to time t , and X_0^t represents the amount of liposomes in a tissue at time t .

2.11. Statistical analysis

Results are expressed as the mean \pm S.D. Analysis of variance (ANOVA) was used to test the statistical significance of differences among groups. Statistical significance in the difference of the means was evaluated by using Student's t -test or Dunnett's test for the single or multiple comparisons of experimental groups, respectively.

3. Results

Several physicochemical characteristics were evaluated for DXR-encapsulated rHSA/PEG liposome and PEG liposome. The average diameters of DXR-encapsulated rHSA/PEG and PEG liposomes were 94.4 ± 6.4 and 95.5 ± 8.1 nm, respectively. DXR encapsulation efficiencies were $97.4 \pm 1.4\%$ and $95.8 \pm 2.1\%$ for rHSA/PEG liposome and PEG liposome, respectively. The amount of rHSA conjugated onto the surface of PEG liposome was 5.3 ± 1.6 $\mu\text{g}/\mu\text{mol}$ total lipid. SDS-PAGE analysis under non-reducing condition revealed that rHSA coupled onto the surface of liposome was exclusively in a monomeric form (data not shown). The release of DXR from the two PEG liposomal preparations was evaluated in an in vitro study for 2 h at 37 °C. The released fraction of DXR was $2.3 \pm 2.6\%$ or $9.3 \pm 5.4\%$ for rHSA/PEG or PEG liposome, respectively.

The in vivo disposition of DXR was evaluated after intravenous injection of free DXR, PEG liposomal DXR or rHSA/PEG liposomal DXR into tumor-bearing rats at a dose of 2.0 mg/kg as DXR. The plasma concentration–time curves

Table 1

Pharmacokinetic parameters of DXR after intravenous administration of free DXR, PEG liposomal DXR or rHSA/PEG liposomal DXR to tumor-bearing rats

	AUC ($\mu\text{g h/mL}$)	CL_{total} (mL/h)	V_d (mL)	k_{el} (h^{-1})
Free DXR	4.52 ± 0.69	131.0 ± 16.1	27.8 ± 5.5	4.86 ± 1.5
PEG liposomal DXR	$33.8 \pm 2.8^{\dagger\dagger}$	$17.9 \pm 1.0^{\dagger\dagger}$	$19.5 \pm 4.4^{\dagger}$	$0.95 \pm 0.17^{\dagger\dagger}$
rHSA/PEG liposomal DXR	$89.7 \pm 12.9^{*\dagger\dagger}$	$7.0 \pm 1.2^{*\dagger\dagger}$	$14.9 \pm 0.9^{\dagger}$	$0.47 \pm 0.08^{*\dagger}$

Each preparation was dosed at 2.0 mg/kg as DXR. AUC, area under the plasma concentration–time curve; CL_{total} , total clearance; V_d , apparent distribution volume; and k_{el} , elimination rate constant, were calculated based on two-compartment model. Results are expressed as the mean \pm S.D. of three experiments. * $p < 0.05$, compared with PEG liposomal DXR. $^{\dagger}p < 0.05$; $^{\dagger\dagger}p < 0.01$, compared with free DXR.

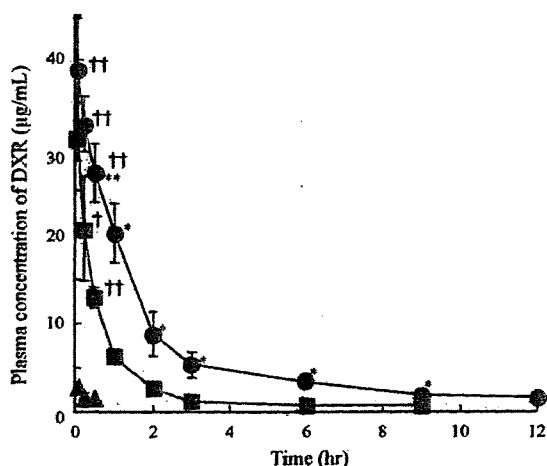


Fig. 1. Plasma concentration–time profiles of DXR after intravenous administration of free DXR, PEG liposomal DXR or rHSA/PEG liposomal DXR to tumor-bearing rats. Each preparation was dosed at 2.0 mg/kg as DXR. Keys: (●) rHSA/PEG liposomal DXR; (■) PEG liposomal DXR; (▲) free DXR. Results are expressed as the mean \pm S.D. of three experiments. * $p < 0.05$; ** $p < 0.01$, compared with PEG liposomal DXR. $^{\dagger}p < 0.05$; $^{\dagger\dagger}p < 0.01$, compared with free DXR.

of DXR after intravenous administration of each preparation were shown in Fig. 1 and pharmacokinetic parameters of DXR were summarized in Table 1. Fig. 1 clearly shows that the injection of rHSA/PEG liposomal DXR exhibited much higher plasma concentrations of DXR compared with free DXR injection, and moreover significantly higher than the injection of PEG liposomal DXR. AUC of DXR for rHSA/PEG liposome ($89.7 \pm 12.9 \mu\text{g h/mL}$) was significantly larger than that for PEG liposome ($33.8 \pm 2.8 \mu\text{g h/mL}$), but both values of AUC were

extensively larger than that for free DXR ($4.52 \pm 0.69 \mu\text{g h/mL}$). Total body clearance (CL_{total}), distribution volume (V_d) and elimination rate constant (k_{el}) of DXR for both PEG liposomal preparations were significantly smaller than those for free DXR. Furthermore, rHSA/PEG liposome provided significantly smaller CL_{total} and k_{el} of DXR than PEG liposome. These results clearly indicate that rHSA-conjugation prolongs the residence time of PEG liposomal DXR in blood circulation.

In the in vivo disposition study, the distribution of DXR after intravenous administration of each preparation was investigated for liver, spleen and heart (Fig. 2), because liver and spleen are main organs for liposome disposition and cardiotoxicity is a critical side-effect of DXR. At 3 h after injection, distribution of DXR into RES was larger for both PEG liposomal preparation than that for free DXR, but the hepatic and splenic clearances were remarkably smaller for both liposome preparations than that for free DXR, suggesting that rHSA/PEG and PEG liposomal preparations would suppress and delay the uptake of DXR into RES. Furthermore, it was revealed that the hepatic and splenic clearances of DXR for rHSA/PEG liposome were significantly smaller than those for PEG liposome, suggesting that the affinity of rHSA/PEG liposome to these organs would be less than PEG liposome. In addition, PEG liposomal preparations significantly suppressed the distribution of DXR into heart compared with free DXR, although there was no significant difference between rHSA/PEG liposome and PEG liposome (Figs. 2 and 3).

To obtain some clue to explain the reason for the lower hepatic and splenic clearances of rHSA/PEG liposomal DXR than PEG liposomal DXR, we measured the amount of serum proteins associated onto the surface of rHSA/PEG or PEG liposomes (Fig. 3). The result clearly demonstrated that the amount

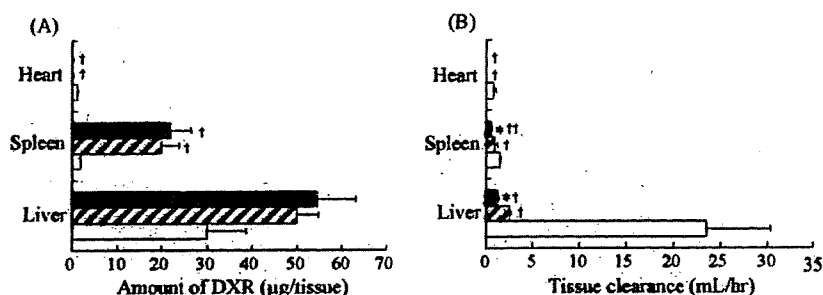


Fig. 2. Tissue distribution of DXR after intravenous administration of free DXR, PEG liposomal DXR or rHSA/PEG liposomal DXR to tumor-bearing rats. (A) Distributed amount of DXR at 3 h after intravenous administration. (B) Tissue clearance calculated according to Eq. (3). Each preparation was dosed at 2.0 mg/kg as DXR. Keys: (□) free DXR; (▨) PEG liposomal DXR; (■) rHSA/PEG liposomal DXR. Results are expressed as the mean \pm S.D. of three experiments. * $p < 0.05$, compared with PEG liposomal DXR in each tissue. $^{\dagger}p < 0.05$; $^{\dagger\dagger}p < 0.01$, compared with free DXR in each tissue.

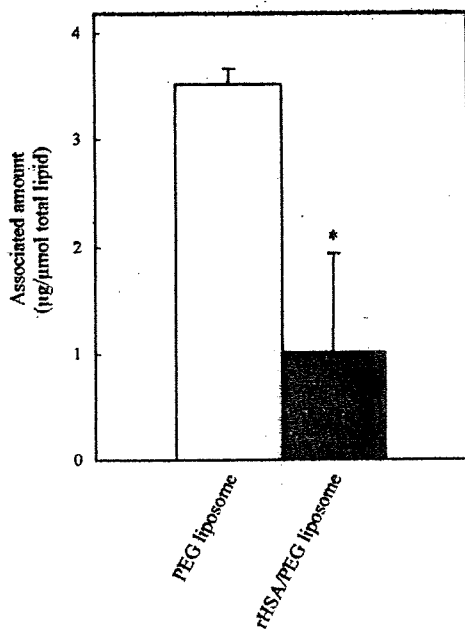


Fig. 3. Amount of serum proteins associated on surface of PEG liposome and rHSA/PEG liposome prepared by SPDP method. Results are expressed as the mean \pm S.D. of three experiments. * $p < 0.05$, compared with PEG liposome. The amount of serum proteins associated with rHSA/PEG liposome was calculated by subtracting the amount of rHSA coupled with liposomes from the total protein amount measured.

of associated serum proteins was significantly reduced by the rHSA-conjugation.

Next, we evaluated the disposition of DXR into tumor tissue at 3 h after intravenous administration (Fig. 4). Significantly increased tumor distribution of DXR was observed for both rHSA/PEG and PEG liposomal preparations compared with free DXR. Furthermore, it should be noted that the amount of DXR in tumor was significantly larger for rHSA/PEG liposome than PEG liposome, demonstrating the usefulness of rHSA-conjugation onto PEG liposome for the better DXR delivery into tumor tissues.

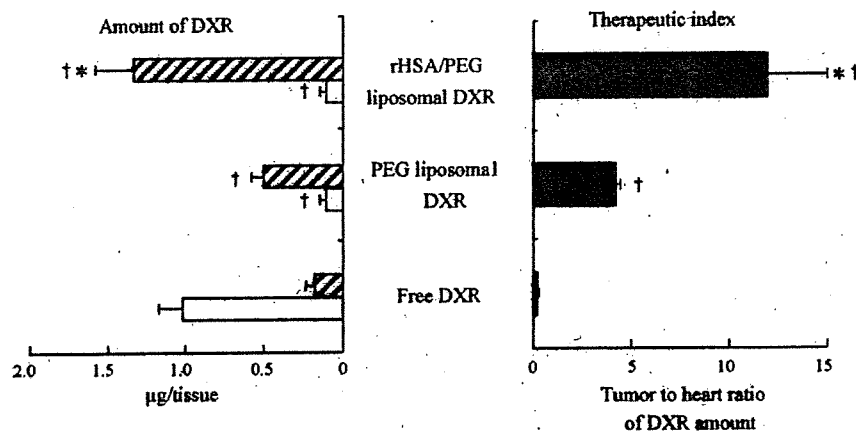


Fig. 4. Amounts of DXR in tumor and heart at 3 h (left) and therapeutic index (right) of free DXR, PEG liposomal DXR or rHSA/PEG liposomal DXR after intravenous administration to tumor-bearing rats. Each preparation was dosed at 2.0 mg/kg as DXR. Therapeutic index was calculated as the tumor to heart ratio of DXR amount. Keys: (▨) DXR amount in the tumor; (□) DXR amount in the heart; (■) therapeutic index of each formulation. Results are expressed as the mean \pm S.D. of three experiments. * $p < 0.05$, compared with PEG liposomal DXR. † $p < 0.05$, compared with free DXR.

The therapeutic outcome of DXR would be evaluated by the balance between its anti-tumor effect and side-effect. Therefore, as a criterion for therapeutic outcome, the therapeutic index, tumor to heart ratio of DXR amount, was calculated for both PEG liposomal preparations and free DXR (Fig. 4). The therapeutic index of rHSA/PEG liposomal DXR was the largest among the three preparations, although PEG liposomal DXR was also significantly better than free DXR. This result clearly demonstrates that rHSA/PEG liposomal DXR would provide better EPR effect for tumor tissues than PEG liposomal DXR.

4. Discussion

Long-circulating particles are promising carriers for passive targeting of drugs into tumors or inflamed tissues, where the integrity of the endothelial barrier is perturbed, via EPR effect (Gabizon and Papahadjopoulos, 1992; Jang et al., 2003). In this study, we tried to evaluate the pharmacokinetics and biodistribution of DXR encapsulated into rHSA-conjugated PEG liposome in tumor-bearing rats.

Several factors such as particle size, charge and lipid composition of liposome have been reported to influence the in vivo fate of liposomes after intravenous administration in rats (Gabizon et al., 1993; Harashima et al., 2002). Among them, the size of liposome is one of the most important factors to influence the EPR effect-driven tumor disposition and the liposomes with the diameter of less than 150 nm are reported to be suitable for the efficient delivery (Harashima and Kiwada, 1996; Drummond et al., 1999; Takeuchi et al., 2001). Therefore, we decided to prepare liposomes with a diameter of 100 nm.

In our previous study, we clearly demonstrated that RSA-conjugated PEG liposome (RSA/PEG liposome), prepared by using carbodiimide, prolonged the blood circulation time of PEG liposome after intravenous administration in rats (Furumoto et al., 2007). Carbodiimide has been widely used as carboxyl- and amine-reactive cross-linker to prepare immunoliposomes (Endoh et al., 1981), polymer-protein conjugates (Dilgimen et al., 2001) and immunomicrospheres (MacAdam et al., 2000).

However, the pH remote loading method is not available for DXR encapsulation into the albumin-conjugated PEG liposome, since carbodiimide can activate carbonyl group only at a low pH region, especially between 3.5 and 4.5 during the first step of reaction (Nakajima and Ikada, 1995). Therefore, in the present study, we chose SPDP as the hetero-bifunctional-cross-linker (Carlsson et al., 1978) to prepare rHSA/PEG liposomes, because the coupling reaction can be conducted under weakly alkaline pH, which makes it possible to perform the pH remote loading method for encapsulating DXR into rHSA/PEG liposomes. SPDP has been widely used for the preparation of disulphide-linked protein-protein conjugates (Moll and Thompson, 1994; Takeoka et al., 2001) and immunoliposome (Barbet et al., 1981; Ishimori et al., 1984; Schwendener et al., 1990). As a result, the encapsulation efficiency of DXR into rHSA/PEG liposomes or PEG liposomes was very high and more than 95% of DXR added was successfully encapsulated.

In vivo disposition studies in tumor-bearing rats revealed that the DXR encapsulation into rHSA/PEG liposomes or PEG liposomes dramatically changed the in vivo disposition characteristics of DXR itself (Fig. 1 and Table 1). Furthermore, rHSA-conjugation onto the surface of liposomes significantly prolonged the blood circulation of DXR compared with PEG liposomal DXR. Taken that the in vitro release study demonstrated that DXR was stably and similarly encapsulated within both liposomal preparations in the presence of plasma and that free DXR was immediately cleared from the blood circulation after injection (Fig. 1), the in vivo disposition characteristics of rHSA/PEG liposomal DXR or PEG liposomal DXR is considered to mainly represent the pharmacokinetics of each PEG liposomes themselves. In addition, rHSA/PEG liposomes significantly reduced the hepatic and splenic clearances of DXR compared with PEG liposomes, although both PEG liposomal preparations remarkably decreased both tissue clearances compared with free DXR (Fig. 2B). Although the disposition amount of DXR in the liver and spleen was larger for both rHSA/PEG and PEG liposomal DXR than that for free DXR, it would be because the distribution of DXR into and the subsequent elimination of DXR from the liver is delayed and prolonged for liposomal preparations, compared with free DXR. The distribution of free DXR to and its subsequent elimination from the liver due to the metabolism, biliary excretion or efflux back to the blood stream are very fast (Colombo et al., 1994; Working and Dayan, 1996). In the case of heart, the amount of DXR at 3 h would reflect the accumulation of DXR in heart (Figs. 2 and 4), considering the very rapid elimination of free DXR from plasma (Fig. 1). Clearance values also confirmed that both PEG liposomal preparations significantly attenuated DXR distribution to heart (Fig. 2B). As Speth et al. (1988) reported that one of the acute or delayed toxicities derived from DXR was cardiac arrhythmias or cardiomyopathy, respectively, the decrease in DXR distribution to heart would be one of the advantages rHSA/PEG liposome can provide.

As described above, in vivo disposition studies clearly indicated the longer circulation of rHSA/PEG liposomal DXR and lower values of tissue clearances for liver and spleen than PEG liposomal DXR. The serum proteins associated onto the surface

of liposomes systematically administered have been suggested to be one of the most important factors to determine their in vivo fate (Drummond et al., 1999; Luigi et al., 2003). Chonn et al. (1992) reported that the amount of serum proteins associated on the liposomes used was inversely related to their circulation half-lives. Our present findings also revealed that less amount of serum proteins was associated on rHSA/PEG liposomes than PEG liposomes (Fig. 3). Since the recognition of surface-associated serum opsonins by their corresponding receptors is mainly a trigger for the receptor-mediated hepatic uptake of liposomes, it is considered that the rHSA-conjugation on PEG liposome suppressed the association of serum proteins including some serum opsonins. Western blotting will be useful to address the possible less-association of typical serum opsonins on rHSA/PEG liposome and will be the subject of our further study.

The movement of liposomes into the tumor interstitium is principally via extravasation through the discontinuous endothelium of the tumor microvasculature (Drummond et al., 1999). Since the maintenance of high blood level or large AUC of particulate drug carriers is one of the driving forces for the efficient extravasation into tumor tissues (Drummond et al., 1999), it can be considered that rHSA/PEG liposomal preparation successfully improved the tumor disposition of DXR over PEG liposomal preparation via EPR effect (Fig. 4). For DXR to exert the anti-tumor effect, DXR must be released and taken up by the surrounding tumor cells. Although DXR is stably incorporated in rHSA/PEG liposomes in plasma, DXR release from the liposome preparations would be enhanced after liposomes are extravasated into tumor tissues, considering that malignant effusions significantly elevated the release of DXR from liposome preparation (Gabizon, 1995). Elucidation of local release profile of DXR in tumor tissues will be the subject for further study.

From the viewpoint of clinical therapeutics, the balance between pharmacological and adverse effects is very important. Therefore, we calculated the therapeutic index defined as the ratio of the amount of DXR delivered to tumor, the site of action, to the DXR amount at potential sites of toxicity, heart (Fig. 4). Therapeutic index was the highest for rHSA/PEG liposomal DXR, suggesting that rHSA-conjugation on PEG liposome would increase the anti-tumor effect as well as the safety of liposomal DXR.

In conclusion, rHSA modification on the surface of PEG liposome significantly prolonged the blood circulation time of PEG liposomal DXR, leading to higher DXR amount in the tumor, but lower level of DXR in heart after intravenous administration. These findings are very useful to optimize albumin-conjugated PEG liposome for the passive targeting of encapsulated drug and for the better therapeutic outcome.

References

- Abraham, S.A., Waterhouse, D.N., Mayer, L.D., Cullis, P.R., Madden, T.D., Bally, M.B., 2005. The liposomal formulation of doxorubicin. *Methods Enzymol.* 391, 71–97.
- Allen, T.M., Hansen, C., Rutledge, J., 1989. Liposomes with prolonged circulation times: factors affecting uptake by reticuloendothelial and other tissues. *Biochim. Biophys. Acta* 981, 27–35.

- Allen, T.M., Hansen, C., Martin, F., Redemann, C., Yau-Young, A., 1991. Liposomes containing synthetic lipid derivatives of poly(ethylene glycol) show prolonged circulation half-lives in vivo. *Biochim. Biophys. Acta* 1066, 29–36.
- Bally, M.B., Nayar, R., Masin, D., Hope, M.J., Cullis, P.R., Mayer, L.D., 1990. Liposomes with entrapped doxorubicin exhibit extended blood residence times. *Biochim. Biophys. Acta* 1023, 133–139.
- Barbet, J., Machy, P., Leserman, L.D., 1981. Monoclonal antibody covalently coupled to liposomes: specific targeting to cells. *J. Supramol. Struct. Cell Biochem.* 16, 243–258.
- Blume, G., Cevc, G., 1990. Liposomes for the sustained drug release in vivo. *Biochim. Biophys. Acta* 1029, 91–97.
- Bolotin, E.M., Cohen, R., Bar, L.K., Emanuel, S.N., Lasic, D.D., Barenholz, Y., 1994. Ammonium sulfate gradients for efficient and stable remote loading of amphipathic weak bases into liposomes and ligandliposomes. *J. Liposome Res.* 4, 455–479.
- Carlsson, J., Drevin, H., Axen, R., 1978. Protein thiolation and reversible protein–protein conjugation. *N-Succinimidyl 3-(2-pyridyldithio) propionate*, a new heterobifunctional reagent. *Biochem. J.* 173, 723–737.
- Chonn, A., Semple, S.C., Cullis, P.R., 1992. Association of blood proteins with large unilamellar liposomes in vivo: relation to circulation lifetimes. *J. Biol. Chem.* 267, 18759–18765.
- Colombo, T., Zucchetti, M., D'Incalci, M., 1994. Cyclosporin A markedly changes the distribution of doxorubicin in mice and rats. *J. Pharmacol. Exp. Ther.* 69, 22–27.
- Dilgimen, A.S., Mustafaeva, Z., Demchenko, M., Kaneko, T., Osada, Y., Mustafaev, M., 2001. Water-soluble covalent conjugates of bovine serum albumin with anionic poly(*N*-isopropyl-acrylamide) and their immunogenicity. *Biomaterials* 22, 2383–2392.
- Dresdale, A., Bonow, R.O., Wesley, R., Palmeri, S.T., Barr, L., Mathison, D., D'Angelo, T., Rosenberg, S.A., 1983. Prospective evaluation of doxorubicin-induced cardiomyopathy resulting from postsurgical adjuvant treatment of patients with soft tissue sarcomas. *Cancer* 52, 51–60.
- Drummond, D.C., Meyer, O., Hong, K., Kirpotin, D.B., Papahadjopoulos, D., 1999. Optimizing liposomes for delivery of chemotherapeutic agents to solid tumors. *Pharmacol. Rev.* 51, 691–743.
- Emree, L., Gelmon, K.A., Lohr, A., Mayer, L.D., Coldman, A.J., Cullis, P.R., Palaitis, W., Pilkiewicz, F., Hudon, N.J., Heggie, J.R., Goldie, J.H., 1993. Chromatographic analysis and pharmacokinetics of liposome-encapsulated doxorubicin in non-small-cell lung cancer patients. *J. Pharm. Sci.* 82, 627–634.
- Endoh, H., Suzuki, Y., Hashimoto, Y., 1981. Antibody coating of liposomes with 1-ethyl-3-(3-dimethyl-aminopropyl)carbodiimide and the effect on target specificity. *J. Immunol. Methods* 44, 79–85.
- Furumoto, K., Yokoe, J., Ogawara, K., Amano, S., Takaguchi, M., Higaki, K., Kai, T., Kimura, T., 2007. Effect of coupling of albumin onto surface of PEG liposome on its in vivo disposition. *Int. J. Pharm.* 329, 110–116.
- Gabizon, A., Papahadjopoulos, D., 1992. The role of surface charge and hydrophilic groups on liposome clearance in vivo. *Biochim. Biophys. Acta* 1103, 94–100.
- Gabizon, A.A., Barenholz, Y., Bialer, M., 1993. Prolongation of the circulation time of doxorubicin encapsulated in liposomes containing a polyethylene glycol-derivatized phospholipid: pharmacokinetic studies in rodents and dogs. *Pharm. Res.* 10, 703–708.
- Gabizon, A.A., 1995. Liposome circulation time and tumor targeting: implications for cancer chemotherapy. *Adv. Drug Deliv. Rev.* 16, 285–294.
- Gabizon, A., Shmeeda, H., Barenholz, Y., 2003. Pharmacokinetics of pegylated liposomal doxorubicin: review of animal and human studies. *Clin. Pharmacokinet.* 42, 419–436.
- Harashima, H., Kiwada, H., 1996. Liposomal targeting and drug delivery: kinetic consideration. *Adv. Drug Deliv. Rev.* 19, 425–444.
- Harashima, H., Ishida, T., Kamiya, H., Kiwada, H., 2002. Pharmacokinetic of targeting with liposomes. *Crit. Rev. Ther. Drug Carrier Syst.* 19, 235–275.
- Ishimori, Y., Yasuda, T., Tsumita, T., Notsuki, M., Koyama, M., Tadakuma, T., 1984. Liposome immune lysis assay (LILA): a simple method to measure anti-protein antibody using protein antigen-bearing liposomes. *J. Immunol. Methods* 75, 351–360.
- Jang, S.H., Wientjes, M.G., Lu, D., Au, J.L.S., 2003. Drug delivery and transport to solid tumors. *Pharm. Res.* 20, 1337–1350.
- Klibanov, A.L., Maruyama, K., Torchilin, V.P., Huang, L., 1990. Amphipathic polyethyleneglycols effectively prolong the circulation time of liposomes. *FEBS Lett.* 268, 235–237.
- Lowry, O.H., Rosebrough, N.J., Farr, A.L., Randall, R.J., 1951. Protein measurement with the Folin phenol reagent. *J. Biol. Chem.* 193, 265–275.
- Luigi, C., Maurizio, C., Franco, D., 2003. From conventional to stealth liposomes. A new frontier in cancer chemotherapy. *Tumori* 89, 237–249.
- MacAdam, A.B., Shafi, Z.B., Marriott, C., Martin, G.P., James, S.L., 2000. Anti-mucus polyclonal antibody production, purification and linkage to the surface of albumin microspheres. *Int. J. Pharm.* 195, 147–158.
- Madden, T.D., Harrigan, P.R., Tai, L.C., Bally, M.B., Mayer, L.D., Redelmeier, T.E., Loughrey, H.C., Tilcock, C.P., Reinish, L.W., Cullis, P.R., 1990. The accumulation of drugs within large unilamellar vesicles exhibiting a proton gradient: a survey. *Chem. Phys. Lipids* 53, 37–46.
- Maeda, H., Wu, J., Sawa, T., Matsumura, Y., Hori, K., 2000. Tumor vascular permeability and the EPR effect in macromolecular therapeutics. *J. Control. Release* 65, 271–284.
- Maruyama, K., Yuda, T., Okamoto, A., Kojima, S., Suginaka, A., Iwatsuru, M., 1992. Prolonged circulation time in vivo of large unilamellar liposomes composed of distearoyl phosphatidylcholine and cholesterol containing amphipathic poly(ethylene glycol). *Biochim. Biophys. Acta* 1128, 44–49.
- Mayer, L.D., Bally, M.B., Cullis, P.R., 1986. Uptake of adriamycin into large unilamellar vesicles in response to a pH gradient. *Biochim. Biophys. Acta* 857, 123–126.
- Moll, T.S., Thompson, T.E., 1994. Semisynthetic proteins: model systems for the study of the insertion of hydrophobic peptides into preformed lipid bilayers. *Biochemistry* 33, 15469–15482.
- Nakajima, N., Ikada, Y., 1995. Mechanism of amide formation by carbodiimide for bioconjugation in aqueous media. *Bioconjug. Chem.* 6, 123–130.
- Schwendener, R.A., Trub, T., Schott, H., Langhals, H., Barth, R.F., Groscurth, P., Hengartner, H., 1990. Comparative studies of the preparation of immunoliposomes with the use of two bifunctional coupling agents and investigation of in vitro immunoliposome–target cell binding by cytofluorometry and electron microscopy. *Biochim. Biophys. Acta* 1026, 69–79.
- Speth, P.A., van Hoesel, Q.G., Haanen, C., 1988. Clinical pharmacokinetics of doxorubicin. *Clin. Pharmacokinet.* 15, 15–31.
- Takeoka, S., Teramura, Y., Okamura, Y., Handa, M., Ikeda, Y., Tsuchida, E., 2001. Fibrinogen-conjugated albumin polymers and their interaction with platelets under flow conditions. *Biomacromolecules* 2, 1192–1197.
- Takeuchi, H., Kojima, H., Yamamoto, H., Kawashima, Y., 2001. Passive targeting of doxorubicin with polymer coated liposomes in tumor bearing rats. *Biol. Pharm. Bull.* 24, 795–799.
- Woodle, M.C., Lasic, D.D., 1992. Sterically stabilized liposomes. *Biochim. Biophys. Acta* 1113, 171–199.
- Working, P.K., Dayan, A.D., 1996. Pharmacological-toxicological expert report. CAELYX (Stealth liposomal doxorubicin HCl). *Hum. Exp. Toxicol.* 15, 751–785.
- Yamaoka, K., Tanigawara, Y., Nakagawa, T., Uno, T., 1981. A pharmacokinetic analysis program (multi) for microcomputer. *J. Pharmacobiodyn.* 4, 879–885.
- Yuda, T., Maruyama, K., Iwatsuru, M., 1996. Prolongation of liposome circulation time by various derivatives of polyethyleneglycols. *Biol. Pharm. Bull.* 19, 1347–1351.



Contents lists available at ScienceDirect

International Journal of Pharmaceutics

journal homepage: www.elsevier.com/locate/ijpharm

Pharmaceutical Nanotechnology

Determinants for in vivo anti-tumor effects of PEG liposomal doxorubicin: Importance of vascular permeability within tumors

Ken-ichi Ogawara^a, Keita Un^a, Keiko Minato^a, Ken-ichi Tanaka^b,
Kazutaka Higaki^a, Toshikiro Kimura^{a,*}

^a Department of Pharmaceutics, Faculty of Pharmaceutical Sciences, Okayama University, 1-1-1 Tsushima-Naka, Okayama 700-8530, Japan

^b Department of Clinical Pharmacy, Shujitsu University School of Pharmacy, Okayama 703-8516, Japan

ARTICLE INFO

Article history:

Received 20 November 2007

Received in revised form 25 January 2008

Accepted 15 March 2008

Available online 27 March 2008

Keywords:

Liposome

Doxorubicin

EPR effect

Tumor vasculature

VEGF

ABSTRACT

To elucidate the determinants of the in vivo anti-tumor efficacy of polyethylene glycol (PEG)-modified liposomal doxorubicin (DOX), we examined its anti-tumor effect against three different tumor cell lines (Lewis lung cancer (LLC), Colon-26 (C26) and B16BL6 melanoma (B16)) in vitro and in vivo. In vitro, LLC was the most sensitive tumor to DOX and liposomal DOX based on the MTT assay. However, the strongest in vivo anti-tumor effect was observed in the C26 tumor-bearing mice. The in vivo accumulation of radio-labelled PEG liposome in the C26 tumor after intravenous injection was significantly larger than in other tumors. The extent of vascularity assessed by immunohistochemical staining of CD31 was not directly related with the tumor accumulation of PEG liposome. On the other hand, Evans blue extravasation and secretion of VEGF in C26 tumors were higher than in LLC tumors, clearly demonstrating that the vascularity permeability was higher within C26 tumors. These results indicated that the vascular permeability within the tumor substantially affects the tumor accumulation of PEG liposome and may be one of the important determinants in the in vivo anti-tumor efficacy of PEG liposomal DOX.

© 2008 Elsevier B.V. All rights reserved.

1. Introduction

The clinical usefulness of the 3-(4,5-dimethylthiazol-2-yl)-2,5-diphenyl tetrazolium bromide (MTT) assay-based in vitro chemosensitivity test is widely recognized to predict patient responses to particular drugs, allowing for the selection of appropriate chemotherapeutic drugs and the avoidance of ineffective drugs, thereby improving patient survival (Tonn et al., 1994; Nakamura et al., 2006). Accumulating knowledge on this assay revealed its usefulness especially to avoid the administration of ineffective chemotherapeutic drugs to patients. However, there are papers reporting the false-positive results of MTT assay-based selection of drugs (Smit et al., 1992; Kratzke and Kramer, 1996; Shaw et al., 1996). These results indicate that not only the in vitro sensitivity of tumor cells isolated from patients toward a given chemotherapeutic drug but also the in vivo disposition characteristics of the drug including its accessibility to tumor tissue would be the important determinants for the therapeutic outcome in the cancer chemotherapy.

Most solid tumors possess unique pathophysiological characteristics that are not observed in normal tissues/organs, such

as extensive angiogenesis, defective vascular architecture and impaired lymphatic drainage/recovery system. Generally, the capillary permeability of the endothelium in newly vascularized tumors is significantly greater than that of normal organs. Many of drug delivery approaches to target tumors take advantage of these unique pathophysiological properties of tumor vasculatures (Maeda et al., 2000). Due to the long circulation time of polyethylene glycol (PEG)-modified liposomes (PEG liposome) and the leakiness of the microcirculation in the solid tumors, PEG liposome containing anticancer drugs has been shown to accumulate preferentially in the tumors (Umezaki et al., 1996; Gabizon et al., 2006; Heyes et al., 2006). This phenomenon known as the enhanced permeability and retention (EPR) effect has been generally observed in many types of solid tumors and provides a great opportunity for passive targeting of liposomal anticancer agents into the tumor tissue (Northfelt et al., 1998; Schmidt et al., 1998). PEG liposomal doxorubicin (Doxil[®], Caelyx[®]) has been approved for the treatment of several types of cancers in Japan, U.S. and Europe. However, the extent of vascularity and permeability of vasculatures within tumors might be different from one tumor to the other. Therefore, these pathophysiological differences in the tumor may result in the different therapeutic effects in the EPR effect-based therapy. In the present study, we prepared the different tumor-bearing mice models (colon adenocarcinoma, C26; Lewis lung cancer, LLC; and B16BL6 melanoma, B16) and analyzed these pathophysiological

* Corresponding author. Tel.: +81 86 251 7948; fax: +81 86 251 7926.
E-mail address: kimura@pharm.okayama-u.ac.jp (T. Kimura).

characteristics of each tumor. Therapeutic effect of intravenously administered PEG liposomal doxorubicin (DOX) was also evaluated in these tumor-bearing mice models to find out determinants for the EPR effect-based *in vivo* anti-tumor effects of PEG liposomal DOX including the *in vitro* sensitivity of these tumor cells to DOX.

2. Materials and methods

2.1. Materials

Distearoyl phosphatidylethanolamine-*N*-[methoxy poly (ethylene glycol)-2000] (PEG-DSPE) and hydrogenated soybean phosphatidylcholine (HSPC) were purchased from NOF Inc. (Tokyo, Japan). Cholesterol (Chol) and [³H] Cholesteryl hexadecyl ether ([³H] CHE) were purchased from Wako Pure Chemical Industry Inc. (Osaka, Japan) and PerkinElmer Life Science Inc. (Boston, MA, USA), respectively. Doxorubicin (DOX), 3-amino-9-ethylcarbazole (AEC) tablets and 3-(4,5-dimethylthiazol-2-yl)-2,5-diphenyltetrazolium bromide (MTT), Dulbecco's modified Eagle's medium (DMEM), RPMI, fetal bovine serum (FBS) and antibiotics were obtained from Sigma (St. Louis, MO, USA). Rat anti-mouse CD31 or rat anti-mouse vascular endothelial growth factor (VEGF) antibody was purchased from BD Biosciences (San Jose, CA, USA) or from R&D Systems (Minneapolis, MN, USA), respectively. Horse radish peroxidase (HRP)-conjugated rabbit anti-rat IgG or goat anti-rabbit IgG was purchased from Zymed Laboratory (San Francisco, CA). All other chemicals were of the finest grade available.

2.2. Cells

LLC, C26 and B16 were kindly provided from Cell Resource Center for Biomedical Research, Institute of Development, Aging and Cancer, Tohoku University (Sendai, Japan). LLC was cultured in DMEM, and C26 or B16 was cultured in RPMI, both supplemented with 100 U/ml penicillin, 100 µg/ml streptomycin, 20 µg/ml gentamicin and 10% heat-inactivated FBS at 37 °C under 5% CO₂/95% air.

2.3. MTT assay

Sensitivity of each type of tumor cells to DOX was evaluated using 3-(4,5-dimethylthiazol-2-yl)-2,5-diphenyltetrazolium bromide (MTT)-based cytotoxicity assay (Mosmann, 1983). Briefly, cell suspension diluted with the corresponding growth medium was added to each well (3000 cells/well) of a 96-well flat bottom microtitration plate (Asahi Techno Glass, Chiba, Japan). All plates were incubated for 12 h at 37 °C in a humidified 5% CO₂ atmosphere. Nine dilutions (0.01–100 µM) of DOX solution or PEG liposomal DOX were added to each corresponding wells in the plate. After incubation for 48 h, each well was washed and rinsed with growth medium. MTT solution (5 mg/ml) was added to each well and the cultures were further incubated for 4 h at 37 °C. The medium containing MTT was removed from the wells and the remaining MTT-formazan crystals were dissolved by adding 100 µl of 0.04 M HCl-isopropanol. After being subjected to sonication in a bath-type sonicator (ASONE Corporation, Osaka) for 15 min, each plate was set into an ELISA plate reader (Bio-Rad, Hercules, CA) and absorbance at 570 nm (test wavelength) and 750 nm (reference wavelength) were simultaneously measured. The absorbance at reference wavelength was subtracted from the absorbance at test wavelength. Results were expressed as percent cell survival, calculated for each DOX concentration by the following formula:

$$\% \text{ cell survival} = \frac{OD_{570, \text{sample}} - OD_{750, \text{sample}}}{OD_{570, \text{control}} - OD_{750, \text{control}}} \times 100 \quad (1)$$

where sample and control mean the cells with and without DOX treatment, respectively. Percent cell survival was plotted against DOX concentration and was fitted with the Hill-type equation (Eq. (2)) (Eghbali et al., 2003; Lim et al., 2004) using the non-linear least-squares regression program MULTI (Yamaoka et al., 1981). The concentration at which 50% of cells survived corresponded to IC₅₀:

$$E = \frac{E_0 \times IC_{50}}{IC_{50} + C} \quad (2)$$

where E or E_0 is the % cell survival with or without DOX treatment, respectively, and C is the final concentration of DOX in each well. Each experiment was performed using three replicated wells for each DOX concentration and carried out independently five times.

2.4. Liposome preparation

Liposomes were prepared as follows. Lipids from chloroform stock solution of HSPC, Chol, and PEG-DSPE were mixed (HSPC:Chol:PEG-DSPE = 56:38:5 by molar ratio) with trace amount of [³H] CHE, and dried under reduced pressure. For liposomes without DOX, the dried lipid film was hydrated with PBS (pH 7.4) under mechanical agitation. Then, the resulting multilamellar preparations were sized by repeated extrusion through polycarbonate membrane filters (Millipore, Bedford, MA, USA) with the pore size of 200 nm followed by further extrusion through the one with 100 nm. For the preparation of DOX-containing liposome, DOX was encapsulated by remote loading method (Haran et al., 1993). In short, after the dried lipid film was hydrated with 250 mM ammonium sulfate (pH 5.4), the resulting liposomes were passed through a Sephadex G-25 column equilibrated with PBS (pH 8.0) to change the pH of the external phase. DOX in PBS (pH 8.0) was added to liposomes at a drug-to-lipid molar ratio of 1:10 and incubated at 60 °C for 1 h. Our preliminary experiments showed that DOX was efficiently encapsulated into liposomes and the loading efficacy was more than 98% reproducibly. Particle sizes of the liposome were determined by dynamic light scattering spectrophotometer (DLS-7000, Otsuka Electronics, Osaka), and were 94.7 ± 9.4 nm and 96.4 ± 14.8 nm for the empty liposome and DOX-containing liposome, respectively.

2.5. Tumor-bearing mice model

Male BALB/c or C57BL6 mice (6–7 weeks) for the inoculation of C26 or LLC and B16, respectively, were purchased from Charles River Laboratories Inc. (Yokohama, Japan) and maintained at 25 °C and 55% of humidity with free access to standard chow and water. To prepare tumor-bearing mice, 1 million tumor cells were subcutaneously injected in the back of mice. Our investigations were performed after approval by our local ethical committee at Okayama University and in accordance with Principles of Laboratory Animal Care (NIH publication #85-23).

2.6. Tissue distribution

Liposome (10 µmol total lipid/kg) containing trace amount of [³H]-CHE was intravenously administered into tumor-bearing mice when the tumor grew up to 500 mm³ in volume. At 48 h after injection, various organs including the liver, spleen, lung, kidney, heart and tumor were excised for the measurement of radioactivity after washed with saline. To solubilize organs, Soluene-350 (Packard instrument Inc., Meriden, CT, USA) was added and incubated for 2 h at 50 °C before neutralized by HCl. Scintillation medium was added to samples, and radioactivity was determined by a liquid scintillation counter (TRI-CARB® 2260XL, Packard instrument Inc.).

2.7. In vivo anti-tumor activity

When the tumor grew up to 500 mm³ in volume, DOX-containing liposome was administered at a dose of 5 mg/kg DOX by intravenous injection through the tail vein. Saline solution was injected into control group. The tumor volume was measured every other day with a caliper in two dimensions, and was calculated using the following equation: volume (mm³) = longer diameter × (shorter one)² × 0.52 (Lee et al., 2005). The results were expressed as % of initial volume for all tumor models. The experiment was terminated when one of the mice in either control or treatment group died. A slope of % of initial volume–time curve, representing the growth rate of each tumor in the treatment group (T), was obtained (day 11–18, 11–24, or 14–28 for LLC, C26, or B16 tumor, respectively) and divided by that in the control group (C) to give an index (T/C) for the in vivo therapeutic effect for each tumor-bearing mouse model.

2.8. Immunohistochemical staining of CD31 or VEGF within the tumor tissue

Tumor tissues were excised from mice when the tumor grew up to 500 mm³ in volume and snap-frozen in isopentane. Acetone-fixed 5-μm thick sections of tumor tissues were prepared with the use of cryostat (CM1850, Leica Microsystems, Wetzlar, Germany). Then, the tumor sections were incubated with rat anti-mouse CD31 antibody or VEGF antibody diluted in PBS containing 5% FBS. This was followed by incubation with horse radish peroxidase (HRP)-conjugated rabbit anti-rat IgG antibody and further incubation with HRP-conjugated goat anti-rabbit IgG antibody. Peroxidase visualization was performed by the conventional staining procedure with 3-amino-9-ethyl-carbazole (AEC, Sigma), and the sections were counterstained with Mayers hematoxylin (Merck, Darmstadt, Germany) according to standard laboratory protocols. In the case of CD31 staining, the staining procedure was followed by the counting of the number of vessels under the microscope in ten independent fields for each type of tumor cells.

2.9. Extravasation of albumin-Evans blue within tumor tissues

Evans blue dissolved in saline (1 mg/mL) was administered into the tail vein of tumor-bearing mice at a dose of 4 mg/kg. Forty-eight hours after intravenous injection, tumors were excised and were snap-frozen. Cross-sections of tumor tissues were prepared as described above and were directly subjected to the observation under the microscope equipped with digital recording system (VH-5000, KEYENCE, Osaka).

2.10. Enzyme-linked immunosorbent assay for VEGF

Tumor tissues with 500 mm³ in volume were homogenized in lysis buffer containing 5% protease inhibitor cocktail (Sigma). VEGF levels were quantified with commercially available enzyme-linked immunosorbent assays (Mouse VEGF ELISA kit, BioSource International, Inc., Camarillo, CA).

2.11. Statistical analysis

Results are expressed as the mean ± S.D. Analysis of variance (ANOVA) was used to test the statistical significance of differences among groups. Statistical significance was evaluated by using Student's *t*-test or Dunnett's test for the single or multiple comparisons of experimental groups, respectively.

3. Results and discussion

To have an optimal in vivo anti-tumor effect in the cancer chemotherapy, many factors that influence the therapeutic outcome should be taken into consideration. Among them, the sensitivity of tumor cells composing a tumor tissue against the anti-cancer drug used is one of the most important factors. Irrespective of the approaches to improve the drug delivery into tumor tissues, the tumor cells with very low sensitivity to a given anticancer drug will not be efficiently killed with the drug. On the other hand, it was reported that anticancer drugs with high sensitivity did not always lead to the good therapeutic outcome (Smit et al., 1992; Kratzke and Kramer, 1996; Shaw et al., 1996).

In the present study, to elucidate the important determinants for the EPR effect-based in vivo anti-tumor effect of PEG liposomal DOX, we first evaluated the sensitivity of each type of tumor cells tested to DOX solution (Fig. 1a). The obtained results revealed that LLC had the smallest IC₅₀ value (0.096 μM) among the three tumor cells studied, indicating that LLC was the most sensitive to DOX solution. B16 tended to show the larger IC₅₀ value (0.213 μM) than LLC, and C26 showed significantly larger IC₅₀ value (0.311 μM) than LLC, suggesting the lower sensitivity to DOX. We also performed the similar study using PEG liposomal DOX (Fig. 1b). It was confirmed that the order of sensitivity of the three tumor cells was the same as that for DOX solution and C26 showed significantly larger IC₅₀ value

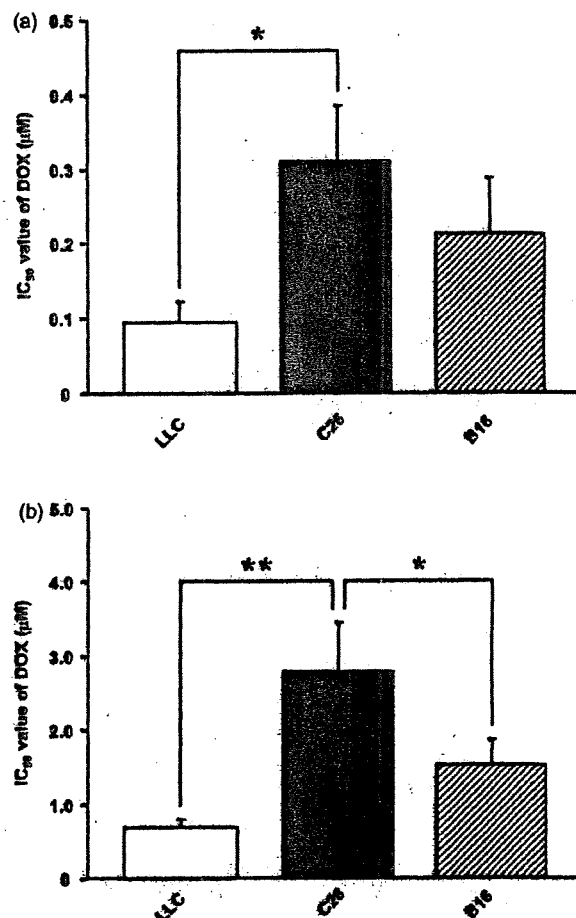


Fig. 1. In vitro sensitivity of Lewis lung cancer (LLC), Colon-26 (C26) and B16BL6 melanoma (B16) cells to DOX solution (a) and PEG liposomal DOX (b). Results are expressed as the mean with the vertical bar showing S.D. of five independent experiments. ***p* < 0.01, **p* < 0.05.

Table 1
Tumor growth rates and T/C values in tumor-bearing mice

	Tumor growth rate (% of initial/day)		T/C
	Control (saline)	PEG liposomal DOX	
LLC	205 ± 72	51.8 ± 18.0	0.35 ± 0.09*
C26	376 ± 89	2.71 ± 7.47	0.07 ± 0.20
B16	123 ± 37	57.2 ± 33.2	0.46 ± 0.27*

Tumor growth rate was estimated as the slope of tumor growth-time curve calculated based on day 11–18, 11–24, or 14–28 for LLC, C26, or B16 tumor, respectively. T/C values were calculated as the ratio of PEG liposomal DOX treated- to control groups in tumor growth rate.

* $p < 0.05$.

** $p < 0.001$, compared with each control group.

$p < 0.05$, compared with C26.

than other tumor cells, suggesting the lowest sensitivity to DOX. The absolute IC_{50} values for PEG liposomal DOX (LLC, 0.68 μ M; C26, 2.5 μ M; B16, 1.4 μ M) were about 10 times larger than DOX solution, reflecting the slow release rate of doxorubicin from PEG liposome.

In vivo anti-tumor effect of PEG liposomal DOX was also studied in the mice bearing C26, LLC or B16 tumor (Fig. 2 and Table 1). Significant in vivo anti-tumor effects of liposomal DOX were observed in all the tumor models studied. On the day when we terminated the experiment, the size of C26 tumor treated with liposomal DOX was much smaller (around 200% of the initial volume) than other tumors investigated (Fig. 2). Since the tumor growth rate was different depending on the type of tumors, we also calculated the index for the in vivo therapeutic effect (T/C) that is independent of the growth rate of each type of tumors, to compare the in vivo efficacy of liposomal DOX and were summarized in Table 1. Calculation of T/C also gave the significantly lower value (0.07 ± 0.20) for C26 tumor-bearing mice than other two tumors (LLC, 0.35 ± 0.09 ; B16, 0.46 ± 0.27). From these results, it was revealed that the strongest in vivo anti-tumor effect was observed in the C26 tumor model, and that the in vivo anti-tumor effect of PEG liposomal DOX was not directly reflecting the sensitivity of tumor cells against DOX.

The in vivo disposition characteristics of intravenously administered PEG liposome must be taken into considerations as one of the crucial factors for the therapeutic outcome of PEG liposomal DOX. It was reported that DOX injected as a solution was so rapidly eliminated from plasma by being excreted into bile and urine and that

the amount of DOX distributed into tumor tissues was very small (Gabizon et al., 1996; Mayer et al., 1989). PEG liposomal preparation can improve the retention of DOX in plasma, but to exert the in vivo anti-tumor effect of PEG liposomal DOX, certain amount of DOX-containing PEG liposome must be extravasated to get into the tumor tissue, and DOX must be released and taken up by the surrounding tumor cells. In plasma, DOX leakage from the liposome with the same lipid composition as those applied in this study was very slow ($T_{1/2} = 100$ h), and the presence of fluid obtained from malignant effusions significantly elevated the release rate (Gabizon, 1995). Therefore, DOX would be mainly released from PEG liposome after the liposome is extravasated within the tumor tissue. Considering the low leakage of DOX from PEG liposome in the blood circulation, the in vivo disposition characteristics of PEG liposomal DOX would be similar to the one of PEG liposome. Therefore, we evaluated the in vivo distribution characteristics of 3H -labeled PEG liposome by measuring radioactivity.

Tissue distribution of PEG liposome at 48 h after intravenous administration was investigated in the mice bearing C26, LLC or B16 tumor of 500 mm^3 in volume (Fig. 3). Tissue distribution of PEG liposome exhibited the similar tendency for each tumor-bearing mice, and it was found that PEG liposome mainly distributed to the liver and spleen irrespective of the type of tumors. On the other hand, the distribution of PEG liposome into tumor was quite different depending on the type of the tumors used, and the disposition amount of PEG liposome in the C26 tumor was significantly and approximately threefold larger than those in the other two tumors. These results suggest that the tumor accumulation of PEG liposome correlates with the in vivo anti-tumor efficacy of PEG liposomal doxorubicin in these tumors.

After its systemic administration, the liposome follows two distinct processes before its accumulation into tumors, i.e., circulation within vessels (blood circulation) and transport across vasculature walls into the surrounding tumor tissues (extravasation). Generally, extravasation of particles in blood circulation is a function of both local blood flow and vascular permeability. One of the factors that influence the local blood flow is the extent of vascularity within the tissue. That is to say, the tissue with numerous vasculatures will receive larger local blood supply. To unravel the mechanism underlying the larger tumor accumulation of PEG liposome in C26 tumor, we evaluated the extent of vascularity in each type of tumor tis-

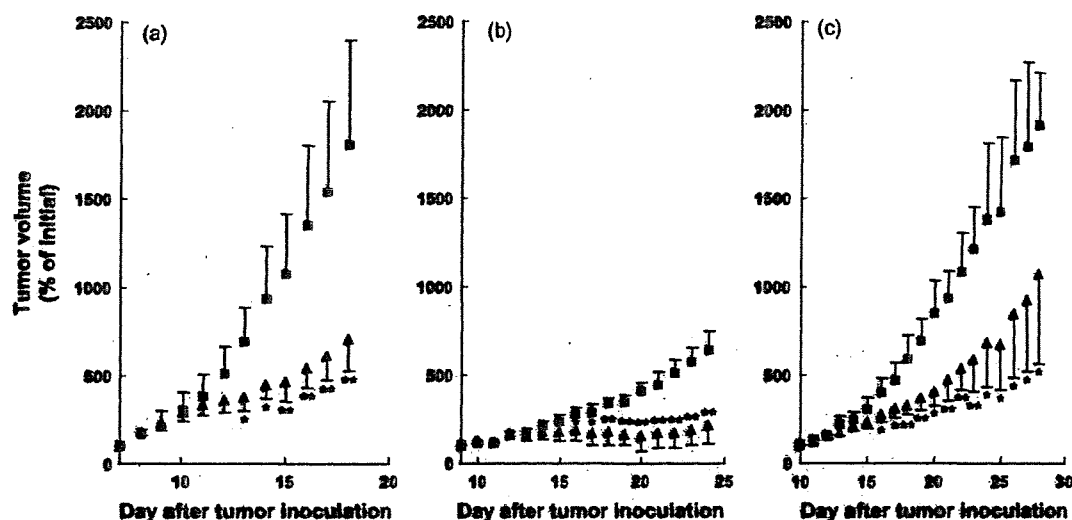


Fig. 2. In vivo anti-tumor effect of PEG liposomal DOX in tumor-bearing mice. Tumor volume was expressed as % of initial volume (around 500 mm^3) for all tumor models. Results are expressed as the mean with the bar showing S.D. of five experiments. * $p < 0.05$; ** $p < 0.01$, compared with saline treatment. (a) LLC-bearing mice; (b) C26-bearing mice; (c) B16-bearing mice. Keys: (■) saline treatment; (▲) PEG liposomal DOX treatment. DOX dose was 5.0 mg/kg.

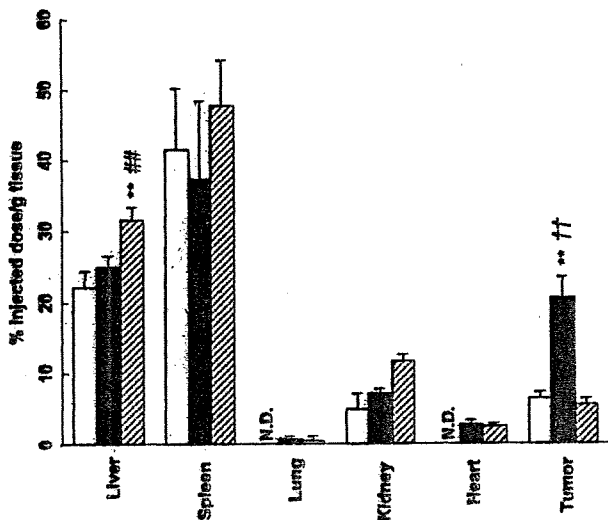


Fig. 3. Tissue distribution of PEG liposomes at 48 h after intravenous administration into tumor-bearing mice. Keys: (□) LLC-bearing mice; (■) C26-bearing mice; (▨) B16-bearing mice. Results are expressed as the mean with the bar showing S.D. of three experiments. ** $p < 0.01$, compared with LLC-bearing mice; ## $p < 0.01$, compared with C26-bearing mice; †† $p < 0.01$, compared with B16-bearing mice. Dose of liposome was $10 \mu\text{mol}$ total lipid/kg.

sue. To visualize the vasculature, cryostat sections were incubated with rat antibody recognizing the mouse endothelial cell marker CD31, followed by the standard staining procedure as described in Section 2. As shown in Fig. 4, in the sections prepared from LLC and B16 tumors, tube-like large vessels were often observed but the numbers of vessels were relatively small (LLC, 28 ± 5 ; B16, 17 ± 6 vessels per field). On the other hand, a lot of tiny vessels (47 ± 6 vessels per field) equally distributed throughout the tumor tissue were observed in C26 tumor.

Besides the extent of vascularity, the permeability of vasculature within the tumor tissue would be one of the important factors influencing the transport of liposome across vasculature walls (Yuan et al., 1995) and may vary considerably depending on the type of tumor models. Several earlier studies demonstrated the differences in the vascular permeability of macromolecules among the tumor tissues used (Graff et al., 2000, 2001; Dreher et al., 2006). Evans blue was utilized to evaluate the vascular permeability of tumor tissues, because the dye spontaneously makes a complex with serum albumin by electrostatic interaction between the sulfonic acid group of the dye and the terminal cationic nitrogens of the lysine residues of albumin (Clasen et al., 1970) and it has, therefore, been generally applied to evaluate the vascular permeability within tumor tissues (Amice et al., 1978; Roberts and Hasan, 1993; Tanaka et al., 2003). Since it was previously reported that the amount of Evans blue

remaining in the blood is negligible at 48 h after its intravenous administration at 10 mg/kg (Graff et al., 2000), we excised tumor tissues at 48 h after intravenous administration in order to discriminate Evans blue extravasated from that in blood vessels. In C26 tumor, the blue color derived from Evans blue was able to be clearly observed equally throughout the tumor (Fig. 5b), suggesting that the permeability of vasculature within C26 tumor would be high and the equal distribution of tiny vasculature throughout the tumor would also be responsible for this observation. On the other hand, in the case of LLC tumor, the blue color was hardly found (Fig. 5a), indicating that the permeability of vasculatures in LLC tumor is very low and that the vascularity is not necessarily a sufficient factor for the efficient intra-tumoral accumulation of PEG liposome. Unfortunately, we were not able to perform the similar study for B16 tumor due to the intrinsic black color of the tissue. Although we did not see any direct relationship between the extent of vascularity (Fig. 4) and the tumor accumulation characteristics of PEG liposome (Fig. 3), the results on Evans blue extravasation obtained for C26 and LLC tumors (Fig. 5) could explain the difference in the tumor accumulation of PEG liposome between the two tumor tissues. That is to say, not only the extent of vascularity within the tumor but also the vascular permeability would be responsible for the accumulation of PEG liposome into tumor tissues. Therefore, the vascular permeability within the tumor would be one of the crucial determinants in the *in vivo* anti-tumor effect of PEG liposomal DOX. To draw more universal conclusion on this issue, however, increasing the number of tumor types investigated would be necessary and will be the subject of our further study. In addition, intra-tumoral distribution pattern of PEG liposome would also be an important factor to determine the *in vivo* anti-tumor effect. Although we did not directly evaluate the intra-tumoral distribution of PEG liposome, we consider that the intra-tumoral distribution of extravasated Evans blue would be reflecting that of PEG liposome. Therefore, it can be considered that the higher permeability of vasculature and the equal distribution of tiny vasculature observed in the case of C26 tumor would be beneficial for the efficient intra-tumoral distribution of PEG liposome. Together with these factors, the difference in the extent of vascularity between central and peripheral parts of tumor tissue and/or the interstitial fluid pressure may vary depending on the type of tumor and would affect the intra-tumoral distribution of PEG liposome.

One of the major factors that influence the vascular permeability within the tumor tissue is VEGF (Kliche and Waltenberger, 2001). To unravel the mechanism underlying the difference in vascular permeability between C26 and LLC tumors, we performed immunohistochemical staining of VEGF within the tumor tissues for the semi-quantification (Fig. 6a and b). As shown in Fig. 6a and b, the higher amount of VEGF in C26 tumor than LLC tumor was detected. Furthermore, the quantification of VEGF amount in each tumor by ELISA demonstrated that approximately eightfold larger

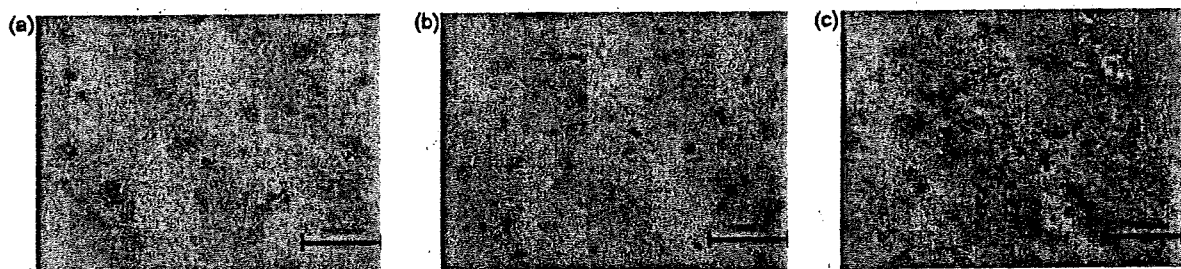


Fig. 4. Immunohistochemical staining of CD31 in each tumor section of LLC (a), C26 (b), and B16 tumors (c). Tumor tissues were excised from mice when the tumor became 500 mm^3 in volume and were snap-frozen. Acetone-fixed $5\text{-}\mu\text{m}$ thick sections of tumor tissues were prepared and then AEC staining was performed for CD31 as described in Section 2. Bar: $100 \mu\text{m}$.